Received: 11 February 2018 | Revised: 14 February 2020 | Accepted: 17 February 2020

DOI: 10.1111/pce.13754

ORIGINAL ARTICLE

Plant, Cell & Environment WILEY

Dynamics of sun-induced chlorophyll fluorescence and reflectance to detect stress-induced variations in canopy photosynthesis

Francisco Pinto[1] | Marco Celesti[2] | Kelvin Acebron[1] | Giorgio Alberti[3,4] | Sergio Cogliati[2] | Roberto Colombo[2] | Radosław Juszczak[5] | Shizue Matsubara[1] | Franco Miglietta[4,6] | Angelo Palombo[7] | Cinzia Panigada[2] | Stefano Pignatti[7] | Micol Rossini[2] | Karolina Sakowska[4,8,9] | Anke Schickling[1] | Dirk Schüttemeyer[10] | Marcin Stróżecki[5] | Marin Tudoroiu[4,10,11] | Uwe Rascher[1]

[1]Institute of Bio and Geosciences, IBG-2: Plant Sciences, Forschungszentrum Jülich GmbH, Jülich, Germany

[2]Remote Sensing of Environmental Dynamics Laboratory, Department of Earth and Environmental Sciences (DISAT), University of Milano-Bicocca, Milan, Italy

[3]Department of Agricultural, Food, Environmental and Animal Sciences, University of Udine, Udine, Italy

[4]Institute of BioEconomy (IBE), National Research Council (CNR), Rome, Italy

[5]Meteorology Department, Poznan University of Life Sciences, Poznań, Poland

[6]FoxLab Joint CNR-FEM Initiative, San Michele all'Adige, Italy

[7]Institute of Methodologies for Environmental Analysis (IMAA), National Research Council (CNR), Rome, Italy

[8]Sustainable Agro-Ecosystems and Bioresources Department, Research and Innovation Centre—Fondazione Edmund Mach, San Michele all'Adige (TN), Italy

[9]University of Innsbruck, Institute of Ecology, Innsbruck, Austria

[10]European Space Agency (ESA), ESTEC, Noordwijk, The Netherlands

[11]University of Natural Resources and Life Sciences, Vienna, Austria

Correspondence
Francisco Pinto, Institute of Bio and Geosciences, IBG-2: Plant Sciences, Forschungszentrum Jülich GmbH, Jülich, Germany.
Email: fr.pinto@cgiar.org

Present address
Francisco Pinto, Global Wheat Program, International Maize and Wheat Improvement Center (CIMMYT), Texcoco, Mexico

Radosław Juszczak, Department of Ecology and Environmental Protection, Laboratory of Bioclimatology, Poznan University of Life Sciences, Poznań, Poland

Anke Schickling, German Aerospace Center, Space Administration, Earth Observation, Bonn, Germany

Abstract

Passive measurement of sun-induced chlorophyll fluorescence (*F*) represents the most promising tool to quantify changes in photosynthetic functioning on a large scale. However, the complex relationship between this signal and other photosynthesis-related processes restricts its interpretation under stress conditions. To address this issue, we conducted a field campaign by combining daily airborne and ground-based measurements of *F* (normalized to photosynthetically active radiation), reflectance and surface temperature and related the observed changes to stress-induced variations in photosynthesis. A lawn carpet was sprayed with different doses of the herbicide Dicuran. Canopy-level measurements of gross primary productivity indicated dosage-dependent inhibition of photosynthesis by the herbicide. Dosage-dependent changes in normalized *F* were also detected. After spraying, we first observed a rapid increase in normalized *F* and in the Photochemical Reflectance

Francisco Pinto and Marco Celesti contributed equally to this work.

This is an open access article under the terms of the Creative Commons Attribution License, which permits use, distribution and reproduction in any medium, provided the original work is properly cited.
© 2020 The Authors. *Plant, Cell & Environment* published by John Wiley & Sons Ltd.

Funding information
Bundesministerium für Bildung und Forschung, Grant/Award Number: 315309/CROP.SENSe.net; Deutsche Forschungsgemeinschaft, Grant/Award Number: SFB/TR 32 project D2; European Space Agency, Grant/Award Number: 4000107143/12/NL/FF/If; H2020 Marie Skłodowska-Curie Actions, Grant/Award Number: 749323

Index, possibly due to the blockage of electron transport by Dicuran and the resultant impairment of xanthophyll-mediated non-photochemical quenching. This initial increase was followed by a gradual decrease in both signals, which coincided with a decline in pigment-related reflectance indices. In parallel, we also detected a canopy temperature increase after the treatment. These results demonstrate the potential of using *F* coupled with relevant reflectance indices to estimate stress-induced changes in canopy photosynthesis.

KEYWORDS
canopy temperature, Dicuran, photochemical reflectance index, photosynthesis, sun-induced chlorophyll fluorescence

1 | INTRODUCTION

Photosynthesis is a highly regulated process that dynamically adapts in order to optimize the use of light while avoiding damage to the photosynthetic apparatus. The quantification of these dynamics is of utmost importance for understanding the responses of photosynthesis to changes in environmental conditions. However, measuring these fluctuations is difficult. They occur at different spatio-temporal scales and they do not necessarily involve changes in the biochemical and biophysical properties of the vegetation. Recently, the passive detection of sun-induced chlorophyll fluorescence (*F*) has been proposed as an approach with a potential to detect dynamics of photosynthesis (Pinto et al., 2016; Rascher et al., 2015; Rossini et al., 2015). Furthermore, the possibility to retrieve *F* from remote sensing platforms provides new opportunities to assess plant photosynthetic functioning at different temporal and spatial scales (Mohammed et al., 2019).

Together with photochemistry and non-photochemical quenching (NPQ), the fluorescence emission is one of the pathways that the excitation energy absorbed by the photosystems can follow. While the NPQ components are physiologically regulated, the emission of fluorescence is merely a physical process that is triggered by an excess of energy in the light harvest complex. Since these three pathways compete for the same excitation energy, the emission of fluorescence can provide information on the status of photochemistry and NPQ (Porcar-Castell et al., 2014). Characterized by two emission peaks centered around 690 and 740 nm, the fluorescence signal is emitted by the chlorophyll *a* molecules in the chloroplasts of higher plants under the prevailing light conditions. At leaf scale, actively induced fluorescence has been used for decades to obtain information on plant photosynthetic activity, helping to elucidate many important features of this process (Papageorgiou & Govindjee, 2004). However, this method is impractical for measurements at the canopy or on larger scales. Through high spectral resolution radiance measurement of the vegetation, the Fraunhofer Line Depth principle (FLD) allows the passive retrieval of fluorescence that arises from the absorption of solar radiation by chlorophylls under natural conditions. This approach opens new perspectives for measuring fluorescence in a wide range of spatio-temporal scales (Meroni et al., 2009). In the last few years, several studies have demonstrated the feasibility of measuring red (F_R) and far-red fluorescence (F_{FR}) from ground platforms (Celesti et al., 2018; Cogliati et al., 2015; Daumard et al., 2010; Magney et al., 2019; Pinto et al., 2016; Rossini et al., 2010, 2016; Zhao et al., 2018), airborne platforms (Bandopadhyay et al., 2019; Damm et al., 2014; Rascher et al., 2015; Rossini et al., 2015) and satellite platforms (Frankenberg, Fisher, et al. 2011; Frankenberg, Butz & Toon 2011; Guanter et al., 2012; Joiner et al., 2011; Joiner, Yoshida, Guanter, & Middleton, 2016). Furthermore, the Fluorescence Explorer (FLEX) mission of the European Spatial Agency will be launched in the near future as the first satellite mission that is specifically intended for fluorescence retrieval from space (Drusch et al., 2017).

The primary interest of the scientific community in the *F* signal has been its potential for improving remote estimations of gross primary productivity (GPP; Byrne et al., 2018; Guanter et al., 2014; Lee et al., 2013; Perez-Priego et al., 2015; Rossini et al., 2010; Schickling et al., 2016; Wieneke et al., 2016, 2018;). Nevertheless, the possibility of using remotely sensed *F* for early detection of stress is also gaining significant attention (e.g., Meroni et al., 2008; Rossini et al., 2015; Song et al., 2018; Xu, Liu, Zhao, Zhao, & Ren, 2018; Zarco-Tejada et al., 2018). Stress events are associated with a reduction in the actual photosynthetic activity of plants, therefore changes in the fluorescence emission are expected to occur before any noticeable effect on leaf reflectance. However, the concurrent operation of the two main de-excitation pathways, that is, the NPQ and photochemistry, complicates the interpretation of the *F* signal in response to stress. There is no universal relationship between photochemistry and *F*, meaning that *F* can either increase or decrease depending on the nature of the stressor and the physiological status of the plants (Porcar-Castell et al., 2014). Ač et al. (2015) performed a meta-analysis of the response of F_R and F_{FR} to different stressors (i.e., temperature, water and nitrogen availability) and observed consistent stressor-specific patterns in *F* values. Recently, Rossini et al. (2015) treated a grass carpet with the DCMU herbicide and demonstrated the feasibility of mapping the two peaks of the chlorophyll fluorescence spectrum from airborne high-resolution radiance spectra. They observed that the variation in the fluorescence signal was linked to herbicide-induced variations in the actual photosynthetic efficiency. Further

development of a mechanistic understanding of the link between *F* and photosynthetic activity under stress conditions requires disentangling the effects from all factors that influence this relationship. Therefore, ancillary information on the NPQ activity and other relevant physiological and physicochemical variables, such as stomatal conductance or pigment composition, must be considered for a proper interpretation of *F* (Alonso et al., 2017; Mohammed et al., 2019; Porcar-Castell et al., 2014; Wohlfahrt et al., 2018). This physiological information can potentially be derived from remote sensing measurements as described in the following.

Numerous spectral vegetation indices have been proposed for remote quantification of leaf pigments. In particular, indices using spectral bands in the red and red-edge regions have proved to be sensitive to variations in chlorophyll content in leaves. Such indices include the Normalized Difference Vegetation Index (NDVI; Rouse, Haas, Schell, & Deering, 1974), the Meris Terrestrial Chlorophyll Index (MTCI; Dash & Curran, 2004) and the Transformed Chlorophyll Absorption in Reflectance Index (Haboudane, Miller, Tremblay, Zarco-Tejada, & Dextraze, 2002). Another technique providing relevant physiological information is thermography. Measurements of canopy temperature have been widely used for remote assessments of stomatal conductance and evapotranspiration (Berni, Zarco-Tejada, Suarez, & Fereres, 2009; Fuentes, De Bei, Pech, & Tyerman, 2012; Li, Zhou, et al. 2013; Panigada et al., 2014; Zarco-Tejada, González-Dugo, & Berni, 2012). On the other hand, the remote quantification of NPQ is particularly challenging. Gamon, Peñuelas, and Field (1992) formulated the Photochemical Reflectance Index (PRI) after observing that the de-epoxidation of violaxanthin to zeaxanthin – a process directly involved in NPQ – causes changes in the leaf reflectance at 531 nm. Strong correlations have been found between PRI and NPQ at leaf and canopy level (e.g., Filella et al., 2009; Filella, Amaro, Araus, & Peñuelas, 1996; Garbulsky, Peñuelas, Gamon, Inoue, & Filella, 2011; Porcar-Castell et al., 2012). However, measurements of PRI at larger vegetation scales can be constrained by the confounding effect of the canopy architecture, sun-target-sensor geometry and background properties (e.g., Garbulsky et al., 2011; Porcar-Castell et al., 2012). Moreover, the temporal relationship between PRI and NPQ might be affected by chlorophyll to carotenoid pigment pool size seasonal dynamics (Gitelson, Gamon, & Solovchenko, 2017).

Many studies have used *F* and other remotely sensed optical indices to successfully detect abiotic or biotic stress (Calderón, Navas-Cortés, Lucena, & Zarco-Tejada, 2013; Calderón, Navas-Cortés, & Zarco-Tejada, 2015; Daumard et al., 2010; Hernández-Clemente, North, Hornero, & Zarco-Tejada, 2017; Panigada et al., 2014; Perez-Priego et al., 2015; Rossini et al., 2015; Song et al., 2018; Wieneke et al., 2016; Xu et al., 2018; Yang et al., 2019; Zarco-Tejada et al., 2012, 2018). However, very seldom these studies use this combination to understand the interplay between the dynamics of *F* and of different physiological and structural plant traits under stress conditions. Xu et al. (2018) demonstrated that ground-based measurements of PRI and canopy temperature are good indicators of diurnal changes in NPQ and in stomata closure, respectively, and together they can be used to explain diurnal changes in F_R and F_{FR} in maize plants subjected to water stress. Perez-Priego et al. (2015) provided new insights regarding the value of *F* and PRI for the estimation of nutrient-induced GPP differences in grassland. Unfortunately, these efforts are not sufficient to build a complete understanding on how different factors may affect the dynamics of *F* under a specific stress. To improve this aspect, further and more robust field studies under different stress conditions are necessary, where optical indices are validated for tracking changes in physiological and structural properties of the vegetation and used to explain dynamics of *F*, and where actual measurements of photosynthesis are conducted for validation.

The main objective of this study was to explore the potential of passive measurements of *F* for detecting stress-induced changes in photosynthetic efficiency at a canopy level over the course of several days after herbicide application. Additionally, we assessed whether canopy temperature, PRI and pigment-related spectral indices could assist with the interpretation of the *F* signal. To induce different levels of stress, we treated plots of homogeneous grass with different doses of Dicuran, an inhibitor of photosynthetic electron transport. A multidisciplinary team conducted concurrent remote-sensing and ground truth measurements of several variables related to photosynthesis regulation under stress conditions. Following the herbicide treatments, a time series of high spectral resolution top of the canopy (TOC) radiance measurements were obtained using airborne and field sensors for the estimation of *F*. Both airborne measurements of the TOC reflectance and *F* were validated against the ground-based measurements. Complementary measurements of surface temperature were conducted using an airborne hyperspectral thermal camera. Concurrently, CO_2 assimilation at canopy level and leaf chlorophyll content were also analyzed to validate the remote sensing assessment of photosynthetic activity. The temporal dynamics of fluorescence, PRI, surface temperature and chlorophyll content are discussed in relation to the action of the inhibitor. The interaction between these variables is further interpreted in order to define a mechanistic understanding of the stress-induced changes in sun-induced chlorophyll fluorescence. This article offers highly valuable information for the future interpretation of the data that will be collected by the FLEX/Sentinel 3 Tandem Mission for Photosynthesis Study and by other future satellite missions capable of monitoring similar variables as those measured in this study.

2 | MATERIALS AND METHODS

2.1 | Study site and experiment design

The experiment took place from June 11 to June 24, 2014, over a homogenous commercial turf grass (*Festuca arundinacea* Schreb. and *Poa pratensis* L.) grown in a farm in Latisana, Italy (Lat: 45.7784° N, Lon: 13.0133° E). In order to inhibit the photosynthetic electron transport, the plants were treated with Dicuran 700 FW (Syngenta AG) which is a commercial formulation of Chlortoluron (3-[3-chloro-p-tolyl]-1, 1-dimethylurea). This herbicide inhibits photosynthesis through the same mechanism of action as the herbicide DCMU

(Weed Science Society of America, 2020). The DCMU has been widely used in photosynthesis and chlorophyll fluorescence studies because it enhances the fluorescence emission by blocking the electron transport in photosystem II (Carter, Jones, Mitchell, & Brewer, 1996; Lichtenthaler & Rinderle, 1988; Schreiber, 1986). The DCMU displaces the plastoquinone (PQ) at the Q_B binding site on the D1 protein of photosystem II reaction center and thereby blocks electron flow from Q_A to Q_B. Three plots of 12 x 12 m^2 were sprayed using a backpack sprayer containing different concentrations of Dicuran: 24 mL/L (plot D24), 6 mL/L (plot D6) and 1.5 mL/L (plot D1.5). Each plot was sprayed with 15 L of herbicide solution. Owing to logistic constraints, the plots were sprayed on two different dates. Plot D24 was treated in the morning of June 12, whereas plots D6 and D1.5 were sprayed on June 19. On each application date, a control plot was sprayed with water, which helped to account for the differences in weather and vegetation conditions between the treatments. While Control 1 was compared with plot D24, Control 2 was used with plots D1.5 and D6. A first set of aerial and ground-based spectral measurements were conducted at each plot before the application of the herbicide, whereas the first post-treatment measurements were performed approximately 3 hr after spraying the plants. Successive measurements were conducted around midday over a period of several days (for details see Table 1). In order to facilitate the comparison of temporal trends between the treatments, all results were expressed in terms of days after treatment. A map of experiment site and plot locations are presented in Figure 1. Both spraying and measurements were conducted under clear sky conditions.

TABLE 1 List of airborne data collected over the experimental site. DOY refers to day of the year

Date	DOY (2014)	Time (UTC + 2) of HyPlant data collection	Time (UTC + 2) of TASI data collection
11-June	162	14:52	14:51
12-June	163	13:40	14:23
13-June	164	13:52	14:09
17-June	168	–	10:17
18-June	169	–	13:20
19-June	170	13:34	11:27
21-June	172	12:57	14:27
22-June	173	12:10	–
24-June	175	11:56	–

2.2 | Aerial hyperspectral and thermal measurements

Aerial hyperspectral images were collected using the HyPlant airborne sensor (Specim, Finland) which was mounted on a Cessna 208 Caravan aircraft. HyPlant is a hyperspectral imager that consists of two push broom modules: the DUAL Channel Imager providing continuous spectral information from 370 to 2,500 nm (full width at half maximum [FWHM]: 3 nm in the visible/near-infrared and 10 nm in shortwave infrared spectral regions), and the Fluorescence Imager (FLUO) which produces data at high spectral resolution (FWHM: 0.25 nm) between 670 and 780 nm. Both imagers were mounted on the same platform, enabling the alignment of their field of view (for details see Rascher et al., 2015). The hyperspectral images were recorded from an altitude of 680 m above ground level resulting in a ground sampling distance of 1 m per pixel in both imagers. The measurements were performed around solar noon (±2 hr) over the course of a total of 13 days (Table 1). The images from the DUAL module were used to compute spectral reflectance and vegetation indices, while the images from the FLUO module were used for the estimation of *F*.

The DUAL images were radiometrically calibrated and georectified using the CaliGeo toolbox (SPECIM, Finland), and the Atmospheric and Topographic Correction model (ATCOR, ReSe Applications Schläpfer) was used to estimate the surface spectral reflectance from these images. Three 9 x 9 m^2 calibration tarps (i.e., white, grey and black) were used to perform an in-flight radiometric calibration of the DUAL images. The tarps were located next to each other

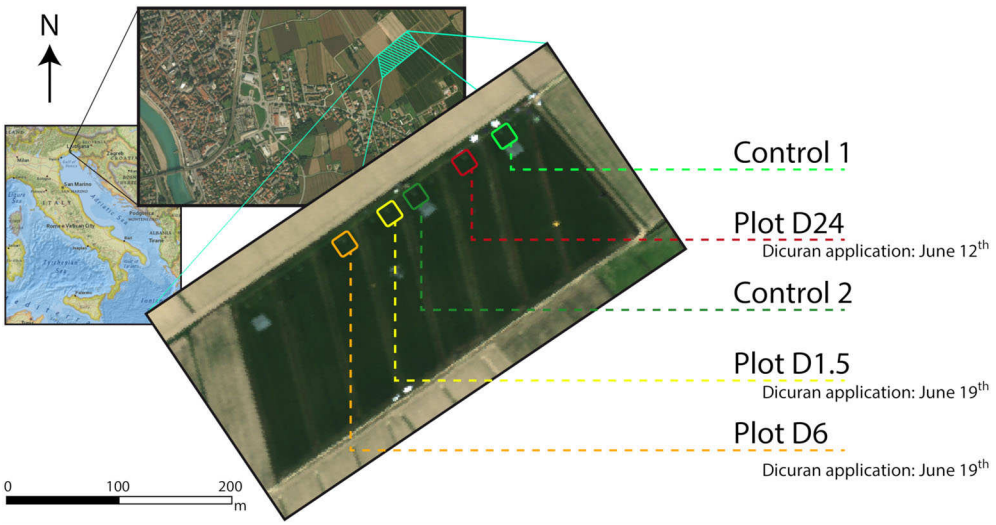

FIGURE 1 Map of the experimental site in Latisana, (northern Italy) and the description of the experimental plots [Colour figure can be viewed at wileyonlinelibrary.com]

in a parking lot located 800 m away from the experimental site, which enabled almost simultaneous ground and aerial measurements of spectral radiance of tarps during each flight line. The tarps spectral reflectance was characterized at each flight through ground-based measurements using a Fieldspec Full Resolution spectroradiometer (Analytical Spectral Devices, Inc., ASD). Twenty measurements were taken over each tarp to account for their spatial variability. A white reference panel (99% Spectralon®, Labsphere, Inc., NH) mounted on a leveled tripod was used to estimate the downwelling radiation needed for the calculation of the spectral reflectance of the tarps. The results of the atmospheric correction were evaluated by computing the root mean square error (RMSE) between the atmospherically corrected data collected with the DUAL module and ground spectra acquired over the tarps. The average RMSE from all wavelengths, calculated using data from all three tarps and all measurement dates, was 0.011, indicating a reliable atmospheric correction (Figure S3).

Three vegetation indices related to pigment concentration and photosynthetic activity were calculated from the DUAL module data: NDVI, MTCI and the PRI (Gamon et al., 1992). For validation, these indices were also estimated from ground level measurements performed as close in time as possible to the airborne sensor overpasses (see Section 2.4). To calculate broadband vegetation indices (i.e., NDVI and MTCI), several bands within each spectral region were averaged to reduce the noise. Table 2 describes the spectral bands used for the calculation of these indices from both platforms.

The images from the FLUO module were radiometrically calibrated and corrected for the point spread function using a sensor characterization and an algorithm developed in-house. Subsequently, the images were georectified using CaliGeo toolbox (SPECIM, Finland) and then used to retrieve fluorescence using the method described in the following section.

Multispectral thermal images were collected using the TASI-600 sensor (ITRES Research Ltd., Calgary, Canada), which is a push broom sensor with 32 spectral bands in the long-wave infrared (8.0–11.5 μm) spectral range. The sensor has a field of view of 40° and FWHM of 0.1095 μm (for details see Pignatti et al., 2011). The TASI-600 data were collected from the afternoon of June 11 until June 21, from an altitude of 900 m above ground level, yielding a ground sample distance of 1 m. The date and time of thermal data acquisition are shown in Table 1.

TABLE 2 Vegetation indices calculated from airborne (HyPlant DUAL) and ground-based (ASD) data

Index	Formulation
NDVI	$\frac{(R_{NIR}-R_{RED})}{(R_{NIR}+R_{RED})}$
MTCI	$\frac{(R_{NIR}-R_{RED-EDGE})}{(R_{RED-EDGE}-R_{RED})}$
PRI	$\frac{R_{530.5}-R_{569.9}}{R_{530.5}+R_{569.9}}$

Abbreviations: MTCI, Meris Terrestrial Chlorophyll Index; NDVI, Normalized Difference Vegetation Index; PRI, Photochemical Reflectance Index; R, reflectance.

NDVI: R_{NIR}, average reflectance between 795 and 809 nm; R_{RED}, average reflectance between 664 nm and 678 nm.

MTCI: R_{NIR}, average reflectance between 747 and 761 nm; R_{RED}, average reflectance between 673 and 687 nm; $R_{RED\text{-}EDGE}$, average reflectance between 700 and 718 nm.

2.3 | Airborne retrieval of sun-induced chlorophyll fluorescence

The fluorescence emitted by the vegetation can be decoupled from the reflected radiation using the FLD principle. In essence, FLD-based approaches exploit the atmosphere absorption bands, where the background solar radiation is strongly diminished and the relative contribution of the fluorescence to the overall vegetation radiance increases (Maier, Günther, & Stellmes, 2003; Meroni et al., 2009; Plascyk, 1975). In this study, we used the improved version of the FLD method (iFLD) proposed by Alonso et al. (2008) to estimate fluorescence in the O_2-A (i.e., at 760 nm; F_{760}) and O_2-B (i.e., at 687 nm; F_{687}) absorption bands.

The iFLD method estimates the fluorescence by building a system of equations where the at-sensor radiance is modeled at two different wavelengths: inside (*i*) and outside (*o*) the absorption band. Following Damm et al. (2015), the radiance measured by an airborne sensor L^{AtS}(L^{AtS}) at a specific wavelength (*j*) over the vegetation can be described by:

$$L_j^{AtS}=\frac{\left\langle E_j^o\cos\theta_{il}\right\rangle}{\pi}\left[\left\langle\rho_{so}^j\right\rangle+\frac{\left(\left\langle\tau_{ss}^j\tau_{oo}^j\right\rangle+\left\langle\tau_{sd}^j\tau_{oo}^j\right\rangle+\left\langle\tau_{ss}^j\tau_{do}^j\right\rangle+\left\langle\tau_{sd}^j\tau_{do}^j\right\rangle\right)R_j}{1-R_j\left\langle\rho_{dd}^j\right\rangle}\right]+\frac{F_j\left(\left\langle\tau_{oo}^j\right\rangle+\left\langle\tau_{do}^j\right\rangle\right)}{1-R_j\left\langle\rho_{dd}^j\right\rangle},j=i,o \quad (1)$$

where E^o is the extraterrestrial solar irradiance, θ_{il} is the illumination zenith angle, ρ_{so} is the path reflectance of the atmosphere, and ρ_{dd} is the spherical albedo of the atmosphere. The terms τ_{ss} and τ_{sd} are the direct and diffuse transmittance of the atmosphere for sunlight, whereas τ_{oo} and τ_{do} represent the direct and hemispherical-directional transmittance in the view direction, respectively. Assuming that the irradiance and the fluorescence emission (*F*) are isotropic, and that the surface reflectance of the vegetation (*R*) has Lambertian behavior, the atmospheric parameters described above (i.e., E^o, ρ_{so}, ρ_{dd}, τ_{ss}, τ_{sd}, τ_{oo} and τ_{do}) can be estimated using the radiative transfer model MODTRAN according to Damm et al. (2015). At this point, only four variables are unknown in the system of equations: the reflectance and the fluorescence inside and outside the absorption band (R_i, R_o, F_i and F_o). Assuming that both reflectance and fluorescence vary linearly between the outside and the inside of the absorption band, the iFLD method relates R_i with R_o and F_i with F_o through the coefficient *A* and *B*, respectively:

$$\left.\begin{aligned} R_o &= A\,R_i \\ F_o\left(\left\langle\tau^o_{oo}\right\rangle+\left\langle\tau^o_{do}\right\rangle\right) &= B\,F_i\left(\left\langle\tau^i_{oo}\right\rangle+\left\langle\tau^i_{do}\right\rangle\right) \end{aligned}\right\} \quad (2)$$

With A and B estimated according to Alonso et al. (2008), the fluorescence inside the O_2-A and O_2-B bands can be calculated using (1) and (2) as:

$$F_i = \frac{AX_i\left(E_o + X_o\left\langle\rho^o_{dd}\right\rangle\right) - X_o\left(E_i + X_i\left\langle\rho^i_{dd}\right\rangle\right)}{\left[A\left(E_o + X_o\left\langle\rho^o_{dd}\right\rangle\right) - B\left(E_i + X_i\left\langle\rho^i_{dd}\right\rangle\right)\right]\left[\left\langle\tau^i_{oo}\right\rangle+\left\langle\tau^i_{do}\right\rangle\right]} \quad (3)$$

with

$$X_j = \left(L^{AtS}_j - \frac{\left\langle E^o_j\cos\theta_{il}\right\rangle}{\pi}\left\langle\rho^j_{so}\right\rangle\right), j = i,o \quad (4)$$

and

$$E_j = \frac{\left\langle E^o_j\cos\theta_{il}\right\rangle}{\pi}\left(\left\langle\tau^j_{ss}\tau^j_{oo}\right\rangle+\left\langle\tau^j_{sd}\tau^j_{oo}\right\rangle+\left\langle\tau^j_{ss}\tau^j_{do}\right\rangle+\left\langle\tau^j_{sd}\tau^j_{do}\right\rangle\right), j = i,o. \quad (5)$$

The atmospheric parameters were simulated at the highest spectral resolution assuming middle latitude summer atmospheric conditions, maritime aerosol model and the default visibility of ATCOR (i.e., 23 km). Next, they were spectrally resampled to meet our sensor configuration taking into account the across-track spectral shift and FWHM. It is worth noting that for parts of Equations (1–4) enclosed in angle brackets, the parameters were first multiplied at their highest resolution and then their product was convolved to meet our sensor configuration. This approach was necessary to compensate for the strong modulation of these parameters by the absorption bands and their strong correlation over finite spectral intervals, both of which result in a direct violation of Beer's law (Damm et al., 2015).

The use of standard atmospheric conditions can lead to inaccurate estimations of some atmospheric parameters that have a great impact on the final fluorescence values. Two empirical corrections were implemented to improve the accuracy of the fluorescence estimation. The first one aimed at obtaining a better estimation of the path reflectance of the atmosphere. For a non-fluorescent target, Equation (1) can be simplified to a two-variable linear equation:

$$L^{AtS}_j = \frac{\left\langle E^o_j\cos\theta_{il}\right\rangle}{\pi}\left\langle\rho^j_{so}\right\rangle + \left[\frac{\left\langle E^o_j\cos\theta_{il}\right\rangle\left\langle\rho^j_{so}\right\rangle\left(\left\langle\tau^j_{ss}\tau^j_{oo}\right\rangle+\left\langle\tau^j_{sd}\tau^j_{oo}\right\rangle+\left\langle\tau^j_{ss}\tau^j_{do}\right\rangle+\left\langle\tau^j_{sd}\tau^j_{do}\right\rangle\right)}{\pi\left(1-R_j\left\langle\rho^j_{dd}\right\rangle\right)}\right]R_j, \quad (6)$$

where L^{AtS}_j and R_j represent the dependent and independent variables, respectively. In cases of two or more non-fluorescent surfaces subjected to the same illumination conditions, it can be assumed that the values of different atmospheric parameters are the same. If the R_j and L^{AtS}_j of each of these non-fluorescence targets are known, and assuming a linear sensor response, a linear regression can be performed to estimate the constants in Equation (6), and therefore to adjust the value of $\rho^j_{so}E^o_j\cos\theta_{il}\,\rho^j_{so}$.($E^o_j$ and $\cos\theta_{il}$ are known since they depend on the date and the time of the day and not on the atmospheric conditions.) The calibration tarps were used for this purpose. The ρ^j_{so} estimated from the tarp measurements was assumed to be constant within the entire scene. A second empirical correction was applied using the effective transmittance correction (ETC) method (Damm et al., 2014; Guanter, 2007) in order to compensate for further inaccuracies and uncertainties in the atmospheric and sensor characterization. In this approach, values of τ^j_{oo} were adjusted across-track using a simple correction coefficient that is calculated from pixels that are known to be non-fluorescent surfaces (e.g., bare soil). Non-fluorescent pixels were detected calculating a normalized difference index using the radiance in the red and near-infrared regions. Pixels with a value below 0.15 were considered as non-vegetation surfaces. Shaded surfaces were discarded from the analysis (for details on the ETC implementation see Pinto et al., 2016).

Since the primary driver of fluorescence emission at canopy level is the incoming radiation, it was necessary to exclude the effects attributed to the natural variations of the incoming radiation from the herbicide treatments effects. Therefore, the fluorescence values were normalized by PAR as follows: Fy* = F/PAR (Rossini et al., 2010), for both the fluorescence at 687 nm (Fy^*_{687}) and at 760 nm (Fy^*_{760}).

2.4 | Ground-based spectroscopy

Downwelling and upwelling radiances were measured over the experimental plots with three portable spectrometers (OceanOptics, Dunedin, FL) operating in the visible and near-infrared regions (Table 3). The spectrometers were housed in a Peltier thermally regulated box (model NT-16, Magapor, Zaragoza, Spain) keeping the internal temperature at 25°C in order to ensure the stability of both the intensity and the spectral information of the measured signal (Meroni & Colombo, 2009). The bare optical fibers (field of view of 25°) attached to the spectrometers were placed at a height of 130 cm above the TOC looking in nadir direction resulting in a measured circular surface of 58 cm diameter. A modified tripod enabled measurements to alternate between a calibrated white reference panel (Labsphere, Inc., North Sutton, NH) and the vegetation (for further details see Rossini

TABLE 3 Summary of the characteristics of the spectrometers used in the study: 'Range' is the spectral range, 'SSI' is the spectral sampling interval, 'FWHM' is the full width at half maximum and 'SNR' is the nominal signal to noise ratio

Spectrometer	Range (nm)	SSI (nm)	FWHM (nm)	SNR
HR4000	400–1,000	0.24	1.00	300:1
QE6500	657–740	0.06	0.25	1,000:1
HR4000	700–800	0.02	0.10	300:1

et al., 2016). The readings over the white panel were used to estimate the downwelling radiation (see Figure S1).

Ground-based spectral data were acquired close to solar noon in order to match the airborne data. Each measurement consisted of three spectral readings recorded sequentially over the white panel, the vegetation and the white panel again. Each of these spectra represented the average of 10 and 3 scans (for the full range and the other two higher resolution spectrometers, respectively) in order to reduce instrumental noise. The number of scans is different because the spectrometers differ in their integration time. The relative variation between the two measurements over the white panel was used as a quality check for the illumination condition stability. Dark current measurements were systematically recorded to eliminate instrument noise from the data. The data were recorded using the dedicated 3S software (Meroni & Colombo, 2009). Five consecutive measurements under stable illumination conditions were taken for each plot.

Ground reflectance measurements acquired in the visible and near-infrared regions were used to compute the vegetation indices indicated in Table 2. The fluorescence was estimated in the red and far-red region (F_{687} and F_{760}) using the spectral fitting method, originally presented by Meroni and Colombo (2006) and recently updated by Cogliati et al. (2015b). The spectral interval used for F_{760} estimation was set from 759.00 to 767.76 nm (i.e., 439 spectral channels), while the spectral range between 684 and 696 nm (i.e., 200 spectral channels) was used for estimating the F_{687}.

2.5 | Canopy gas exchange chamber measurements

The non-steady-state flow-through chamber system was used to estimate CO_2 and H_2O exchange in the plots. The net ecosystem exchange (NEE) and the ecosystem respiration (R_{eco}) were derived directly from measurements using a transparent and an opaque chamber, respectively (chamber's dimension: 0.78 x 0.78 x 0.50 m^3). Chambers were equipped with a set of air-mixing fans, a temperature sensor (T-107, Campbell Scientific) and a vent to maintain pressure equilibrium between the chamber and the ambient air in accordance with Juszczak et al. (2013). In addition, a PAR quantum sensor (SKP215, Skye Instruments, UK) was installed on top of the transparent chamber. No cooling system was used in order to avoid biasing H_2O fluxes. Gas concentration changes in the chambers were measured with the LI-840 infrared gas analyzer (Li-COR, Lincoln, NE) housed in a portable control box (for details see Juszczak, Uździcka, Stróżecki, & Sakowska, 2018). During measurements, chambers were fixed to the soil frames (one per experimental plot) inserted into the soil on June 5. The closure time of the transparent chamber was no longer than 1 min to avoid overheating of the chamber headspace and 2 min for the opaque chamber.

The measured CO_2 concentrations were corrected for water dilution in accordance with Perez-Priego et al. (2015). CO_2 and H_2O fluxes were calculated based on gas concentration changes over the closure time using the linear regression type as described in Juszczak et al. (2013). Fluxes were calculated based on the first 30–40 s of measurements, corresponding to the highest regression slopes, in order to avoid underestimation of the fluxes due factors such as gas saturation, in accordance with Hoffmann et al. (2015). Due to a very small proportion of chamber volume occupied by plants (Figure S2), the reduction in the effective chamber volume was considered negligible and plant volume was not incorporated into flux calculations.

The NEE measurements were taken just after reflectance and fluorescence measurements on the same plots and followed by R_{eco} measurements. The amount of CO_2 assimilated by plant photosynthesis (i.e., GPP) was calculated as the difference between consecutively measured NEE and R_{eco}. The light use efficiency was calculated as the ratio between GPP and PAR. Only measurements taken around solar noon (±1.5 hr) were used to calculate mean midday values and were analyzed in this study.

2.6 | Airborne retrieval of surface temperature

Thermal images were geometrically and radiometrically corrected with the GEOCORR and the RADCORR software (ITRES Research Ltd., Calgary, Canada). An additional code developed by the Italian National Research Council (CNR IMAA) was used to remove blinking pixels (Santini et al., 2014). The atmospheric correction of spectral radiances was executed by applying the in-scene atmospheric compensation (ISAC) algorithm (Young, 1998). This procedure was chosen as it is commonly used for in-scene atmospheric thermal data correction and because it requires only the at-sensor radiance data as input to estimate the upwelling radiance and transmissivity of the atmosphere. The temperature retrieval was then performed by using the temperature emissivity separation methods (TES), applying the normalization emissivity method and selecting an emissivity of 0.98 for the pixel with the maximum brightness temperature (Li, Zhou, et al. 2013). In order to validate the TASI-600 retrieved temperature, the simultaneously ground-measured temperature of a swimming pool located in the Latisana test site test was recorded using a thermocouple. The difference between the ground-based and the average temperature retrieved with TASI was 0.2 K. To reduce the white noise introduced by the TES algorithm in the thermal images, the brightness temperature was retrieved for each flight line using a linear regression between the TES temperature images and the integrated radiance images. To account for the changes in the meteorological conditions during the experiment, the difference in temperature between each treated plot and the closest control plot (ΔT) was used to study the effect of Dicuran on the canopy temperature.

2.7 | Pigment concentration

Leaf samples were collected for laboratory measurements of chlorophyll (Chl) and carotenoid (Car) content. Seven samples per plot were collected starting from 10 hr until 7 days after the treatments. Each sample consisted of three to five leaves. Fresh samples were weighed

(fresh weight; FW) for later estimation of Chl content in $\mu g\, g^{-1}$ FW. The leaf material was harvested, placed in 2 ml safe lock reaction tubes (Safe Lock, Eppendorf, Germany), frozen in liquid nitrogen and stored at −80°C until pigment extraction. The extraction of Chl *a*, Chl *b* and Car was carried out using a mixture of 1,000 ml of 100% acetone buffered with 20 g of magnesium hydroxide carbonate ($\sim 4MgCO_3 \cdot Mg[OH]_2 \cdot 5H_2O$) that was stored at 4°C. Hereafter, this solution is referred to as acetone. The samples were ground using 200 µl of acetone and two steel balls of 5 mm diameter in a mixer mill (MM200, Retsch, Germany) for 2 min at 30 rps and at room temperature. The extract was pipetted into a new 2 ml reaction tube. The grinding jar and the steel balls were washed with acetone and this solution was used to fill the sample up to 500 µl. The samples were then centrifuged at 13,000 rpm for 5 min at 4°C. The excess solution was then measured in the spectroradiometer (Uvikon XL, BIO-TEK Instruments, Winooski, VT) using a 1 cm glass cuvette. The concentration of Chl and Car ($\mu g \cdot ml^{-1}$) was calculated following Lichtenthaler and Buschmann (2001).

3 | RESULTS

3.1 | CO_2 assimilation

Table 4 shows the results of gas exchange measured in all the treatments around noon on the day of the Dicuran application and in the subsequent 3 days in the case of plot D24. Plots D24 and D6 showed a significant reduction of GPP and LUE after the application compared to the control plot, whereas in D1.5, the GPP reduction was not statistically significant. The extent of photosynthetic inhibition was positively correlated with the dose of Dicuran. While the lowest concentration (i.e., 1.5 ml/L) only induced a non-significant decline in GPP of about 17% on the first day, 6 ml/L reduced GPP by nearly 35%. The largest decrease in GPP (nearly 90%) was observed in plants treated with the highest herbicide dose (24 ml/L; plot D24). The LUE, which was calculated as GPP/PAR, showed a similar behavior. GPP tended to remain low, with an exception on the second day after the treatment, when an increase of GPP, and thus LUE, was detected. The Dicuran application also affected the respiration rate. An increased respiration was measured in plots D24 and D1.5 immediately after the treatment. In contrast, respiration in plot D6 showed no significant difference to the control plot. The herbicide treatment did not have a significant effect on evapotranspiration (i.e., H_2O fluxes) during the day of application. In the following days however, the treatment in plot D24 resulted in a decrease in evapotranspiration. The decrease in H_2O fluxes in D24 was not statistically significant on Day 2 and Day 3 due to the gradual decline found in the corresponding control plot from Day 0 to Day 3.

3.2 | TASI surface temperature

The aerial thermal images in dicated an increase in canopy temperature in all treated plots. Figure 2 shows the development of the temperature difference (ΔT) between the treated plots and their adjacent control area. The ΔT increased gradually during the 5 days following the application before it started to decrease towards the end of the experiment. The plots treated with lower doses also showed an

TABLE 4 Effect of the application of Dicuran on CO_2 fluxes measured around midday

DAT	Treatment	GPP ($\mu mol\ CO_2\ m^{-2}\ s^{-1}$)	LUE ($\mu mol\ CO_2\ \mu mol\ PAR^{-1}$)	R_{eco} ($\mu mol\ CO_2\ m^{-2}\ s^{-1}$)	NEE ($\mu mol\ CO_2\ m^{-2}\ s^{-1}$)	F_H_2O ($mmol\ H_2O\ m^{-2}\ s^{-1}$)
0[a]	Control	−43.70 ± 1.2	0.02333	17.96 ± 1.5	−25.74 ± 1.1	9.97 ± 2.6
	Dicuran 1.5 ml	−36.34 ± 6.5	0.01878**	27.86 ± 3.9**	−8.48 ± 2.6**	11.44 ± 0.2
	Dicuran 6 ml	−28.20 ± 3.0**	0.01494***	13.50 ± 2.7	−14.69 ± 0.4	9.30 ± 1.7
0[a]	Control	−38.79 ± 6.3	0.01971	14.91 ± 1.5	−23.89 ± 5.0	11.88 ± 0.9
	Dicuran 24 ml	−4.33 ± 1.4***	0.00220***	22.08 ± 1.0***	17.75 ± 2.4***	12.43 ± 1.1
1	Control	−41.18 ± 3.3	0.02041	20.45 ± 2.9	−20.73 ± 0.7	9.97 ± 0.6
	Dicuran 24 ml	−8.91 ± 1.6***	0.00452***	23.33 ± 1.9	14.43 ± 2.4***	7.67 ± 1.2**
2	Control	−45.32 ± 5.1	0.02106	22.27 ± 5.2	−23.05 ± 1.1	8.01 ± 0.3
	Dicuran 24 ml	−18.85 ± 4.8***	0.00871***	33.53 ± 2.6	14.68 ± 2.3***	4.70 ± 1.15
3	Control	−45.81 ± 8.0	0.02377	21.67 ± 7.4	−24.15 ± 0.7	6.18 ± 0.8
	Dicuran 24 ml	−3.33 ± 0.8***	0.00160***	11.58 ± 0.8**	8.25 ± 0.9***	5.53 ± 1.19

Note: Positive flux indicates CO_2 emission to the atmosphere, whereas, negative flux indicates CO_2 uptake. Values represent the average and standard deviation of different measurements taken ±1.5 hr around solar noon. The time of the measurements is expressed in days after treatment (DAT), where DAT 0 correspond to the first post application measurement taken only 3 hr after the treatment with Dicuran.

Abbreviations: DAT, decimal days after treatment; GPP, gross primary productivity. Amount of CO_2 assimilated by the vegetation (NEE − Reco). R_{eco}, ecosystem respiration. Amount of CO_2 released to the atmosphere. NEE, net ecosystem exchange (GPP + R_{eco}). LUE, light use efficiency (GPP/PAR). F_H_2O, water vapor fluxes.

[a]Measurements taken a few hours after the application of Dicuran.

**$p < .05$. ***$p < .001$.

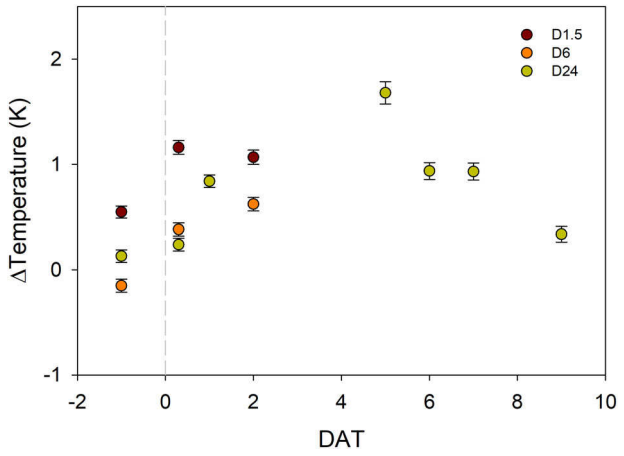

FIGURE 2 Dynamic changes of canopy temperature in plots treated with different doses of Dicuran. Values represent the difference in temperature (in *K*) between the treatment plots and their adjacent control. Vertical bars represent the standard error of the mean difference (n = 32 pixels) [Colour figure can be viewed at wileyonlinelibrary.com]

increase in temperature, albeit with larger effects found in D1.5 than in D6.

3.3 | Changes in spectral vegetation indices as result of the Dicuran action

Airborne images revealed changes in the spectral reflectance of canopies treated with Dicuran (Figure 3). In treated plots, especially in plot D24, vegetation indices related to green biomass and leaf pigment concentration, such as NDVI and MTCI, showed a sustained decrease in comparison to the control (Figure 4a,d). This was also observed in ground-based top-of-canopy measurements (Figure 5b,e). Generally, there was a good correlation between the NDVI and MTCI values calculated from both platforms throughout the whole experiment (Figure 4c,f).

Before the treatments, the plots showed values of NDVI around 0.84 and 0.90 for airborne and ground-based data, respectively (Figure 4a,b). The NDVI in D24 did not show significant variations immediately after the treatment, and it only started to decrease gradually 2 days after the Dicuran application. It reached about 90% of the control by Day 6, but it remained constant in the control plot. The dynamics of NDVI in plots treated with lower doses followed a similar pattern to the control plots. Negative effects of Dicuran were also evident for MTCI, which exhibited larger and more significant changes than NDVI following the application (Figures 3 and 5d,e). In both airborne and ground-based data, MTCI in plots D1.5 and D6 decreased to levels similar to those in D24. Nevertheless, the ground-based data showed a continuous decrease towards the end of the experimental period, while the airborne measurements indicated MTCI stabilization 3 days after the application. Again, the control plots did not show significant variations in MTCI during the course of the experiment, always keeping higher values than the treated plots. These changes in MTCI during the experiment were closely related to the changes in leaf Chl *a* content (R^2 = .749; p < .01; Figure 5), suggesting that MTCI is a good proxy to detect changes in chlorophyll content induced by Dicuran.

Substantial changes were also detected for PRI in the ground and airborne data (Figures 3 and 4g,h). The treated plots showed a noticeable increase of PRI 3 hr after the application of Dicuran; D24 caused the largest increase while D6 the smallest. In all the treatments, this initial increase was followed by a decrease, which was more clearly manifested in the ground-based than in the airborne data (Figure 4h, g). After 6 or 7 days, the PRI values of the ground-based measurements were substantially lower in the treated plots than in the control plots. Ground-based and airborne PRI values showed a significant correlation throughout the experiment (Figure 4i). Considering that the calculation of PRI is based on the wavelengths in the visible part of the spectrum (Table 2), we examined the relationship between PRI and leaf pigments. A significant negative correlation (R^2 = .33; p < .05) was found between PRI and the Car to Chl ratio (Car/Chl; Figure 5).

3.4 | Response of sun-induced chlorophyll fluorescence

Dynamic changes of Fy* in response to the treatment with Dicuran were detected by both airborne (Figures 6 and 7a,d) and ground-based platforms (Figures 7b,e). Before the application of the herbicide, the aerial images depicted similar Fy* (i.e., $Fy^*_{687} \approx 1.5 \times 10^{-5}$ and $Fy^*_{760} \approx 4.3 \times 10^{-5}$) for all the plots. A substantial and rapid increase in Fy* was observed in all the treated plots shortly after the application. In plot D24, airborne measurements showed increases in Fy^*_{687} and Fy^*_{760} by nearly 50% and 90%, respectively, only 3 hr after the herbicide was applied (Figure 7a,d). Likewise, the ground-based measurements detected an increase of approximately 145% and 120% for Fy^*_{687} and Fy^*_{760} in D24, respectively (Figure 7b,e). This increase in Fy* coincided with the increase in PRI (Figure 4g,h). In the following days, the Fy* in plot D24 decreased (Figure 7b,e) in parallel with the decrease in NDVI, MTCI and PRI (Figure 4b,e,h). The Fy* returned to the initial pre-treatment levels after 7 days.

Some differences were observed between the aerial and ground observations in the recovery rate of Fy^*_{687} after the peak. In this regard, it is worth mentioning that the retrieval of fluorescence at 687 nm is prone to noise due to the shallower O_2-B band. This can result in some inconsistencies between the data from both platforms. In spite of these limitations, the correlation between ground and aerial data was high for both F_{687} and F_{760} (Figure 7c,f).

The dynamics of Fy^*_{687} and Fy^*_{760} showed similar temporal patterns in plot D24 (i.e., a rapid increase, a peak approximately 3 hr after the treatment and a steady decrease from Day 2 onwards). However, in the plots treated with lower doses of Dicuran, there were some differences in the temporal changes between both fluorescence peaks (Figure 7a,b,d,e). In these plots, Fy^*_{687} behaved similarly to plot D24, but Fy^*_{760} peaked only 2–3 days after the treatment. This difference

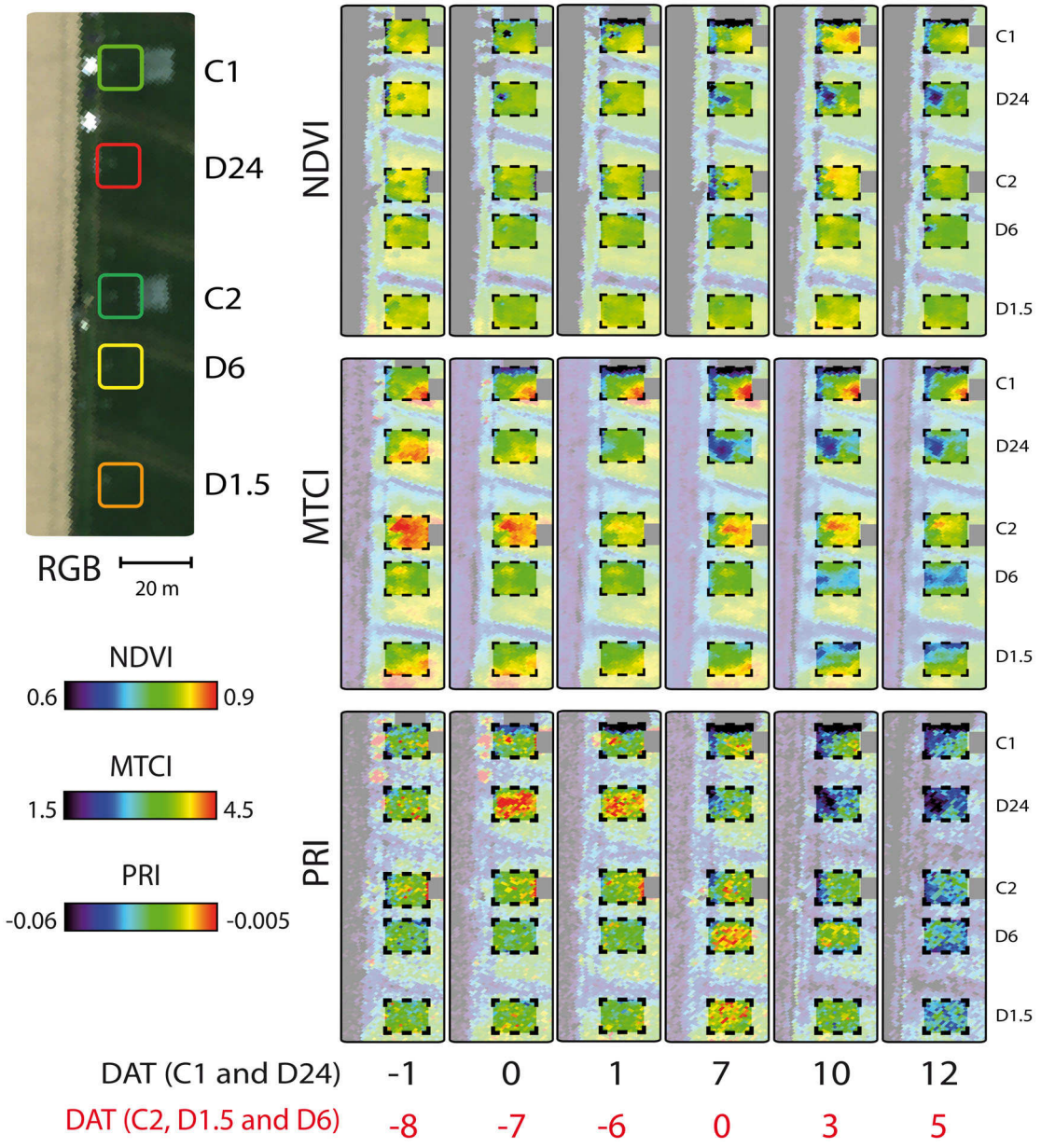

FIGURE 3 Representation of airborne images showing the dynamics of vegetation indices NDVI, MTCI and PRI in plots treated with three different doses of Dicuran: 24 ml/L (D24), 6 ml/L (D6) and 1.5 ml/L (D1.5). Plot D24 was treated on June 12 and plots D6 and D1.5 were treated on June 19. The time of the measurements is expressed in days after treatment (DAT), where DAT 0 correspond to the first post-application measurement taken only 3 hr after the treatment with Dicuran. Scale bar: 20 m. MTCI, Meris Terrestrial Chlorophyll Index; NDVI, Normalized Difference Vegetation Index; PRI, Photochemical Reflectance Index

becomes more evident when comparing changes in Fy* versus PRI (Figure 8). The peak of PRI coincided with the peak of Fy^*_{687} in all the plots, but in the following days Fy^*_{760} continued increasing (at a lower rate) in plots D6 and D1.5 despite the drop of PRI.

4 | DISCUSSION

In this study, we aimed to improve the understanding of how sun-induced chlorophyll fluorescence fluctuates under a stress condition and how these dynamics relate to changes in the photosynthetic function. The use of Dicuran induced a quick and well-characterized effect in the photosynthetic apparatus. Dicuran is a herbicide that blocks the binding site of Plastoquinone A in photosystem II (PSII) and therefore inhibits the photosynthetic electron transport to photosystem I (PSI; Rossini et al., 2015; Schreiber, 1986; Van Rensen, 1989). It has been observed that certain grass species have different levels of resistance to chlorotoluron (Ducruet, Sixto, & Garcia-Baudin, 1993; Hall, Moss, & Powles, 1995; Hyde, Hallahan, & Bowyer, 1996). This resistance is not explained by a change in the

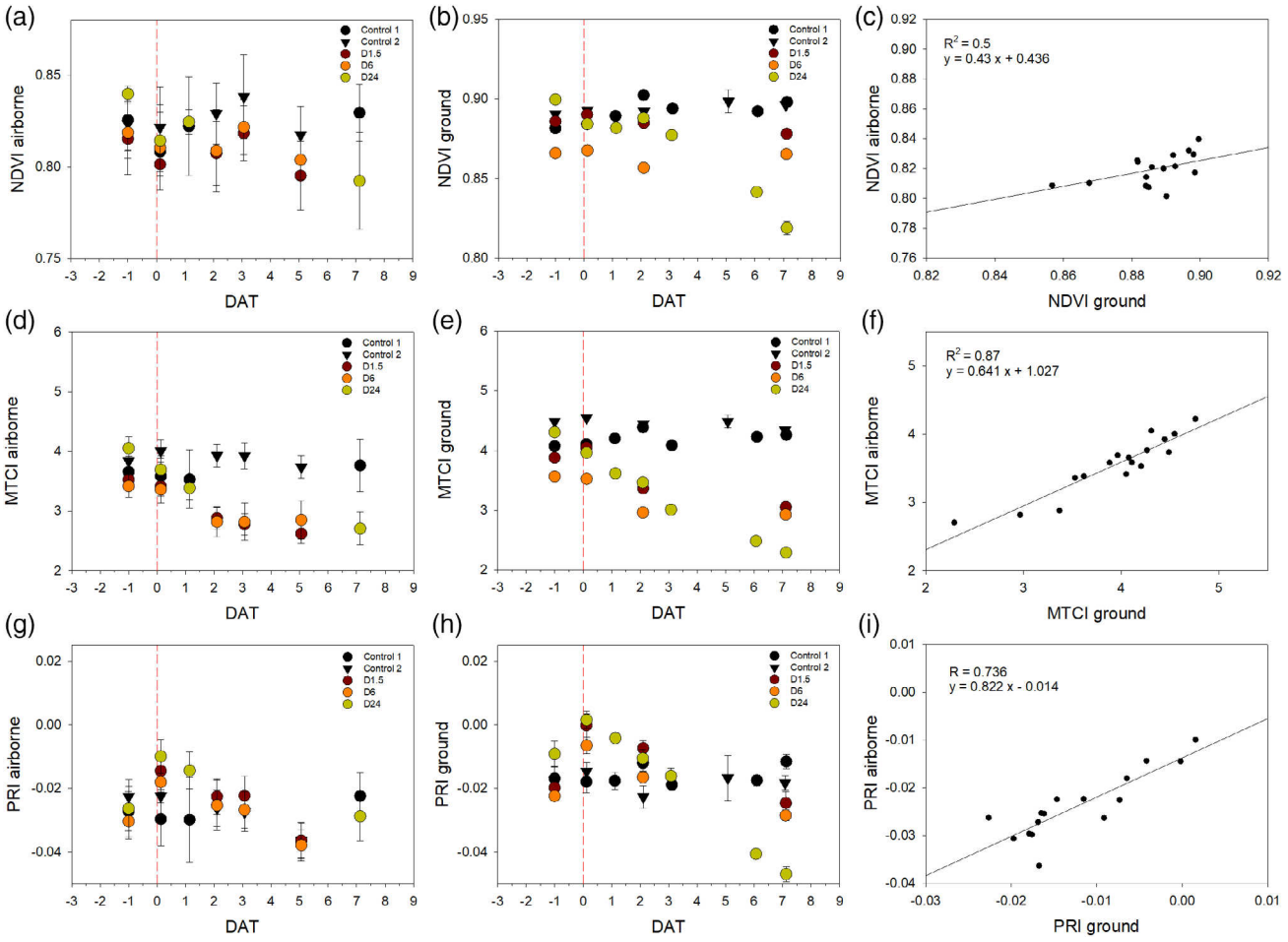

FIGURE 4 Dynamic changes of vegetation indices during the experiment for all the plots estimated from airborne (a, d and g) and ground-based measurements (b, e and h). NDVI (a and b), MTCI (d and e) and PRI (g and h). Correlation between airborne and ground observations for NDVI (c), MTCI (f) and PRI (i). Vertical bars in airborne data represent the standard deviation of pixels within each plot. Vertical bars in ground-based data represent the standard deviation of the different point measurements taken around noon for each plot. The time of the measurements is expressed in decimal days after treatment (DAT), where DAT 0 represent the moment of the application. Data values obtained before the treatment were grouped at DAT −1 for clarity of the results. MTCI, Meris Terrestrial Chlorophyll Index; NDVI, Normalized Difference Vegetation Index; PRI, Photochemical Reflectance Index [Colour figure can be viewed at wileyonlinelibrary.com]

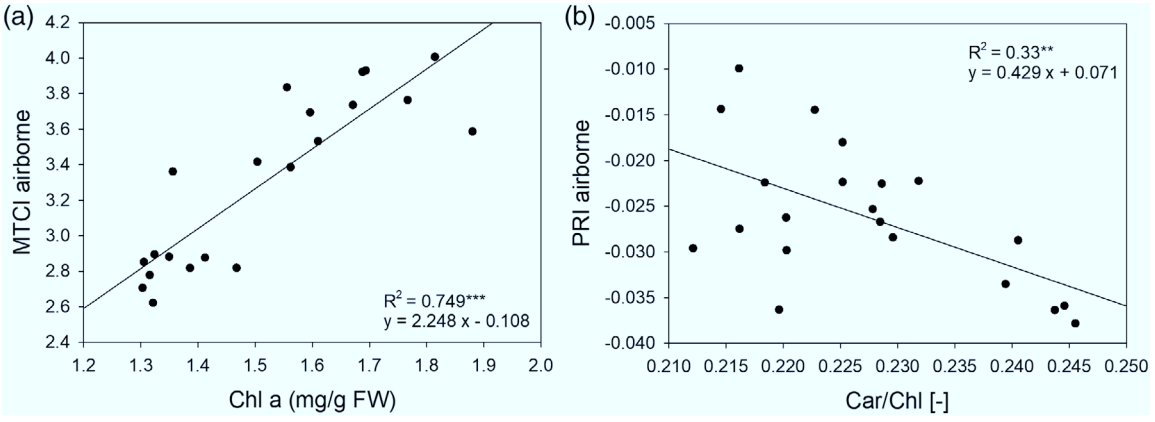

FIGURE 5 Relationship between the concentration of Chl *a* and the MTCI (a), and between the ratio carotenoids/chlorophyll (Car/Chl) and the PRI (b). The MTCI and PRI were estimated from the spectral reflectance measured with the airborne DUAL module. Data points represent the measurements of all plots for all the dates where airborne data coincided with leaf sampling. Significance: **p* < .05, ***p* < .01, ****p* < .001. MTCI, Meris Terrestrial Chlorophyll Index; PRI, Photochemical Reflectance Index

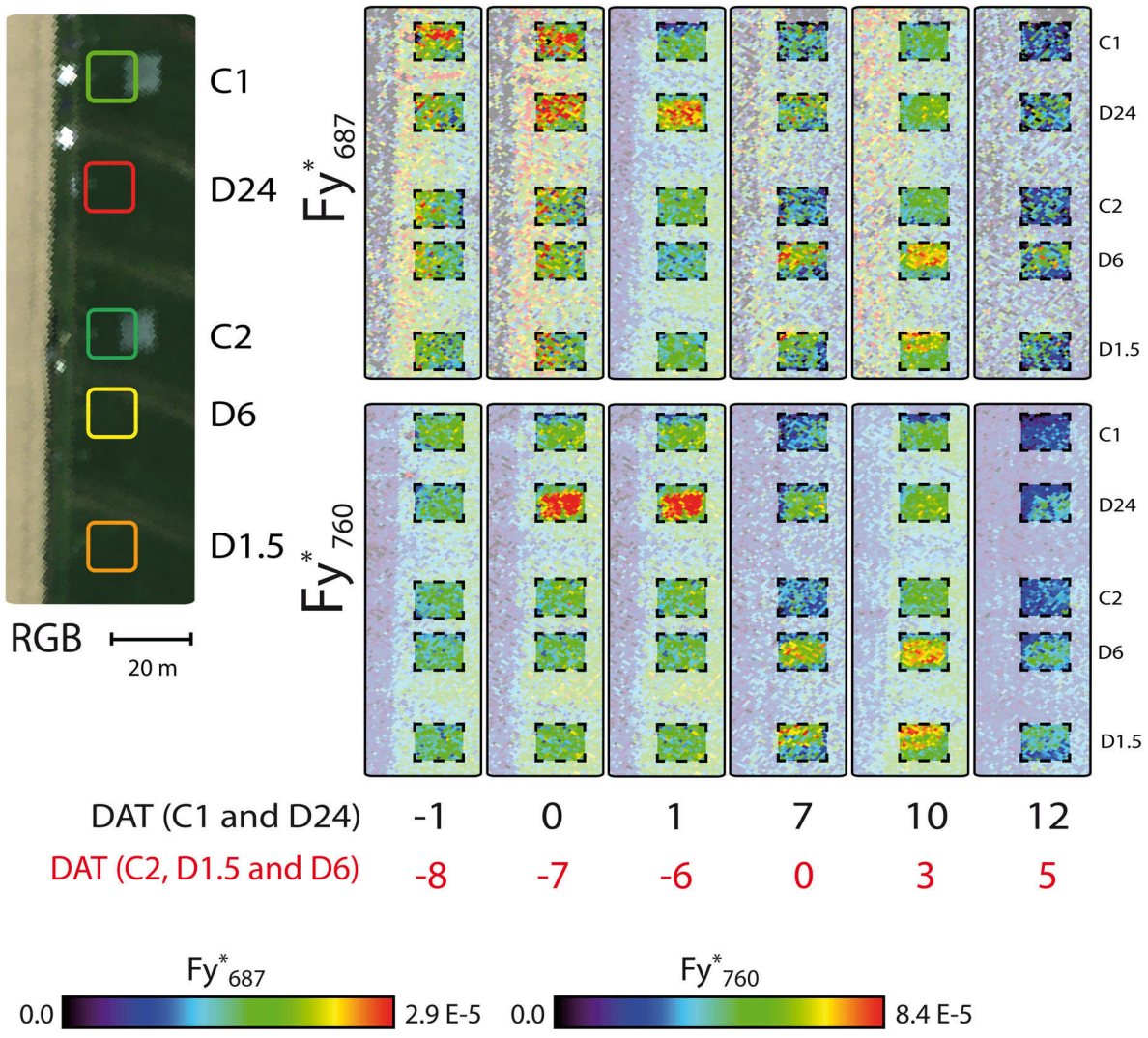

FIGURE 6 Representation of airborne images showing the dynamics of normalized sun-induced chlorophyll fluorescence at 687 nm (Fy^*_{687}) and at 760 nm (Fy^*_{760}) in plots treated with three different doses of Dicuran: 24 ml/L (D24), 6 ml/L (D6) and 1.5 ml/L (D1.5). Plot D24 was treated on June 12 and plots D6 and D1.5 were treated on June 19. The time of the measurements is expressed in days after treatment (DAT), where DAT 0 correspond to the first post-application measurement taken only 3 hr after the treatment with Dicuran. Scale bar: 20 m

herbicide active site, but rather by the capacity to metabolize this molecule. Consequently, PSII remains equally sensitive to the action of this herbicide in both resistant and non-resistant species (Hall et al., 1995). We did not investigate the resistance to Dicuran of the species used in our study and to the best of our knowledge, no information is available in the literature. A difference in Dicuran resistance between these species would mainly have an effect on the magnitude of the fluorescence peak observed in the first hours after the application, and on the change rate of pigment degradation and fluorescence on the following days. Unfortunately, the nature of our observations would not allow the separation of the response of each species in such a mixed turf and the plot was considered as a homogeneous vegetation unit. However, given the management of the turf, we can safely assume that all the plots had the same grass composition. Therefore, the conditions of the experiment and the results are still valid to draw general conclusions on the fluorescence behavior in relation to biochemical and biophysical changes in the photosynthetic apparatus. Other stress factors that may occur under natural environmental conditions generally induce a different response of fluorescence emission. For example, water deficiency or heat stress usually induces a reduction in photosynthetic efficiency, but typically also an increase of the NPQ which results in a decline in fluorescence emission (Ač et al., 2015; Dobrowski, Pushnik, Zarco-Tejada, & Ustin, 2005; Flexas et al., 2002; Song et al., 2018). On the other hand, fluorescence emission increases under chilling temperatures (Ač et al., 2015; Agati, 1998). Biotic stresses can also induce changes in fluorescence. Zarco-Tejada et al. (2018) observed lowered fluorescence values when olive trees were infected with *Xylella fastidiosa*. Nevertheless, despite the differences that might exist between the action of Dicuran and natural stressors, some of

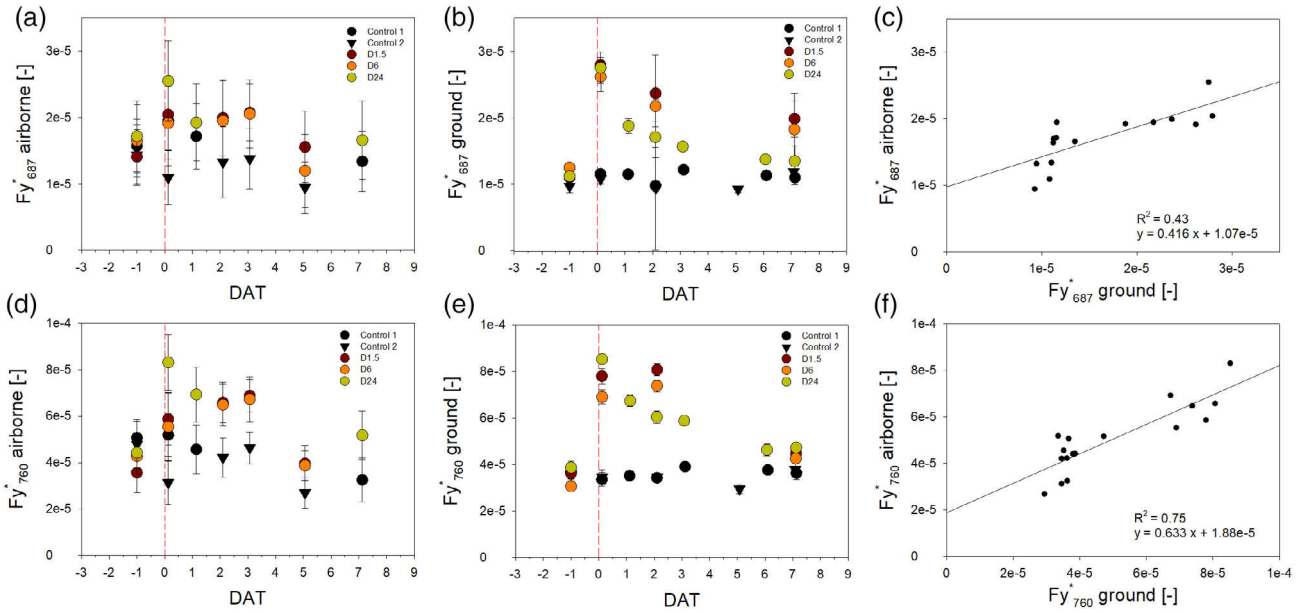

FIGURE 7 Dynamic changes of normalized sun-induced chlorophyll fluorescence (Fy*) during the experiment for all the plots estimated from airborne (a and d) and ground-based measurements (b and e). Fy^*_{687} (a and b) and Fy^*_{760} (d and e). Correlation between airborne and ground observations for Fy^*_{687} (c) and Fy^*_{760} (f). Vertical bars in airborne data represent the standard deviation of pixels within each plot. Vertical bars in ground-based data represent the standard deviation of the different point measurements taken around noon for each plot. The time of the measurements is expressed in decimal days after treatment (DAT), where DAT 0 represent the moment of the application. Data values obtained before the treatment were grouped at DAT −1 for clarity of the results [Colour figure can be viewed at wileyonlinelibrary.com]

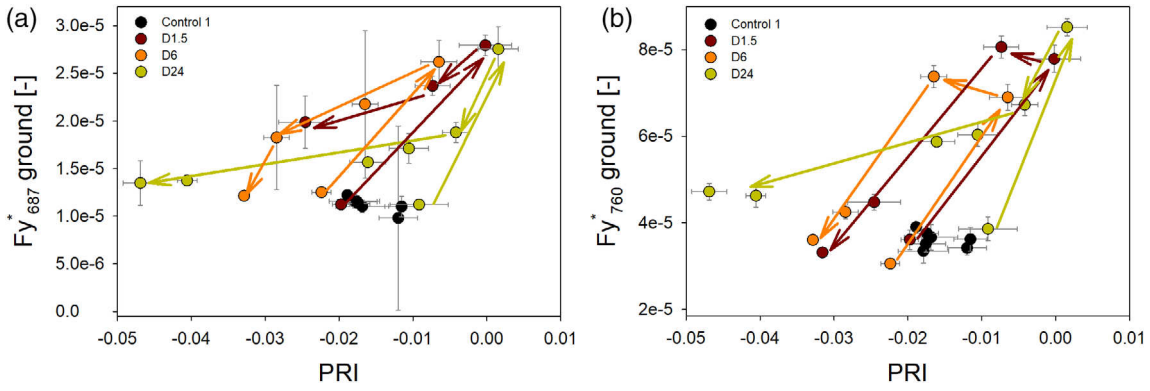

FIGURE 8 Relationship in time between PRI and the normalized sun-induced chlorophyll fluorescence measured at 687 (Fy^*_{687}) and 760 nm (Fy^*_{760}). The arrows indicate the time series and trends of the measurements in each plot. The error bars represent the standard deviation [Colour figure can be viewed at wileyonlinelibrary.com]

the alterations in the processes involved in photosynthesis are comparable.

Only a few hours after the application of Dicuran, a rapid increase in fluorescence was measured by both aerial and ground-based platforms. The rapid changes seen in the fluorescence signal, but not seen in the reflectance indices related to leaf pigments, confirms that the retrieved fluorescence signal dynamically responded to changes in photosynthetic function while changes in vegetation greenness were minimal shortly after the application of the herbicide. Moreover, these changes in fluorescence coincided with the detection of large reductions in CO_2 assimilation rates and LUE together with an increase in canopy temperature. This suggests that the treated plants closed their stomata in the days following the application.

The relationship between LUE and Fy* was different when observing the behavior of individual plots in time. For instance, plot D24 showed a decrease of Fy* following the peak observed immediately after the application, whereas LUE and GPP tended to remain low and constant. This implies that the decrease in Fy* after its peak could not be explained only by a change in LUE. We found a progressive decrease in leaf Chl content (through MTCI) and PRI in Dicuran-treated plots during the course of the experiment. These observations may indicate that the mid-term decreases of fluorescence resulted

from a reduction of photosynthetic pigments and the activation of non-photochemical energy dissipation mechanisms. The reduction in the chlorophyll content may be a direct consequence of photodamage and part of the photoprotective mechanisms to reduce the absorbed radiation (Osmond, 1994; Ridley, 1977; Ruban & Horton, 1999). Interestingly, despite the decrease in NDVI and MTCI observed in sprayed plants, the Fy* remained higher in the treated compared to the control plots towards the end of the experiment. Two possible reasons could explain this behavior. One possibility is that at this point the effect of the pigment breakdown and accompanying reduction in absorbed PAR, is still lower compared to the effect of the blockage of the electron transport chain. Therefore, treated plants would still emit more fluorescence than in their initial state. A second possibility is that since top leaves were subjected to higher PAR and probably to higher levels of Dicuran, the pigment degradation started from the top layer. This would result in a higher light penetration and consequently a higher contribution to the total fluorescence by the middle and bottom layers of the canopy. An increase in the fluorescence emitted by the lower layers, plus a reduction of the red fluorescence re-absorption, could explain why Fy* remained higher in treated plots compared to control plots a few days after the treatment. Unfortunately, we do not have sufficient data to draw a more conclusive explanation of this phenomenon and further studies on the vertical profiles of physiological parameters are required to verify the above hypotheses.

It has been reported that the PRI is a good estimator of NPQ (Gamon et al., 1992; Panigada et al., 2014; Schickling et al., 2016). However, it has been shown to be sensitive to changes in the content of pigments in leaves, in particular to the ratio Car/Chl (Garbulsky et al., 2011; Panigada et al., 2009). In our experiment, the rapid increase of PRI observed immediately after the application of the Dicuran suggests a change in NPQ activity at this time point. Under non-stress conditions, the PRI would normally decrease with increasing light towards midday because of the activation of the xanthophyll cycle, a major component of the NPQ (Gamon et al., 1992; Müller, Li, Niyogi, & Muller, 2001; Murakami & Ibaraki, 2019). However, this decrease in PRI during a dark–light transition is prevented when DCMU (with a similar mechanism of action to Dicuran) inhibits the violaxanthin de-epoxidation by preventing the trans-thylakoid pH gradient (Gamon et al., 1990; Murakami & Ibaraki, 2019). This would explain the high values of PRI observed around noon in plots treated with Dicuran. To confirm this, we replicated the experiment on a smaller scale under controlled conditions and within a shorter time frame. Plants treated with Dicuran showed a fast increase in PRI during the first 30 min, whereas PRI remained low in the control plants (Figure S4). It is worth mentioning that the data displayed in Figure S4 was collected only to validate the field and airborne data collected in the main experiment. Any further analysis on this data obtained at a shorter time scale is beyond the scope of this article.

The initial increase in PRI observed in treated plots suggests a partial inhibition of the xanthophyll-mediated NPQ, an effect that would contribute to the increase of the normalized fluorescence observed immediately after the treatment. Furthermore, the lower peaks of PRI observed in plots treated with lower doses of Dicuran may indicate a lower degree of NPQ inhibition. This could explain the lower peaks observed for Fy* in this plot, especially for Fy^*_{760}. The later decline of PRI in all the treated plots could be explained by a reactivation of the NPQ mechanisms during the days following the initial peak of Fy*. However, under these conditions, the decrease of Fy* and PRI after their peaks can be better explained by the pigment degradation inferred from NDVI and MTCI measurements and confirmed by the laboratory pigment analysis. In our measurement, nearly 40% of the variation of PRI was explained by changes in the Car/Chl ratio, confirming the findings of Panigada et al. (2009). A decrease of this ratio driven by the degradation of chlorophyll would result in a lower PRI (Garbulsky et al., 2011). Similarly, the emission of fluorescence would be reduced in all wavelengths due to a lower absorption of PAR.

It has been reported that the difference between the kinetics of Fy^*_{687} and Fy^*_{760} can provide valuable information to elucidate the level at which the stress is affecting photosynthesis (Ač et al., 2015; Buschmann, 2007; Wieneke et al., 2016). In this experiment, we observed that in the lower dose treatments the initial rise of Fy^*_{687} was quenched faster than Fy^*_{760}. This rapid decrease of Fy^*_{687} coincided with the decrease of PRI suggesting an effect of the combined action of NPQ and the degradation of chlorophyll. In the case of Fy^*_{760}, the peak was observed after the PRI started to decrease. One reason for this could be that the Dicuran action directly affects the short-term and mid-term regulatory mechanisms of light harvesting in the PSII where the F_{687} originates. Hence, any evolution of the stress would modulate this signal almost instantaneously. On the other hand, F_{760} is emitted by both photosystems. The fraction of F_{760} emitted from PSI would only change indirectly and therefore more slowly after the Dicuran application. Further analysis of this would require an improvement in the red fluorescence measurement uncertainties plus complementary data, such as fluorescence emission and the quantum efficiency at each photosystem using active fluorometry.

In summary, the changes in fluorescence emission that we observed under stress conditions resulted from the interaction of different factors regulating photosynthesis. Understanding these effects is crucial for the use of sun-induced fluorescence as a proxy for remote observations of photosynthesis. The set of parameters measured during this study proved to be useful to infer changes in a series of interlinked processes that affect fluorescence emission and the functioning of photosynthesis during stress. The sudden increase of Fy* reflects the immediate inhibition of photosynthetic electron transport in light reactions. Additionally, non-photochemical mechanisms for energy dissipation were inhibited as indicated by the rapid increase in PRI. Presumably, this happened because the absence of electron transport increased the pH in the thylakoid lumen thereby inhibiting the de-epoxidation of violaxanthin into zeaxanthin (Müller et al., 2001). This makes the photosynthetic apparatus susceptible to photodamage. A degradation of chlorophyll occurred due of the excess of energy as well as being part of the strategy to reduce the absorbed radiation. At the same time, the blockage of the photosynthetic light reactions prevented the reduction of $NADP^+$ to NADPH and the formation of ATP. This resulted in an almost complete

downregulation of CO_2 fixation by Rubisco, which was clearly reflected in a decrease in carbon assimilation detected by our gas exchange measurements. This would also result in an accumulation of reactive oxygen species and stromal calcium in the chloroplasts. This may be part of a signaling mechanism for stomatal closure (Wang, He, Guo, Tong, & Zheng, 2016). Both the increase of canopy temperature and the decrease in transpiration rate observed in the treated plots support the idea that stomata partially closed after the application of Dicuran. In the following days, the gradual decline in chlorophyll content (inferred from the changes in MTCI) contributed to a decrease in the fluorescence signal. Although the GPP data showed some signs of recovery in the plot treated with the highest dose of Dicuran, the drastic decline of Fy* and PRI towards the end of the experiment were better explained by a long-term breakdown of chlorophyll and possibly to irreversible damage in the photosynthetic apparatus. Indeed, by the end of the experiment the plants treated with the highest dose were killed by the action of the herbicide.

5 | CONCLUSIONS

In this experimental study, we explored the use of sun-induced fluorescence together with other remote sensing approaches as a proxy to detect stress-induced limitations in photosynthetic activity in large-scale vegetation. The herbicide Dicuran was used to simulate a stress event that triggered changes in different components of the photosynthetic apparatus. We showed that no single measurement parameter was sufficient to reflect the dynamic changes of CO_2 uptake rate. Fluorescence measured at both 687 and 760 nm could clearly tracked functional impairment of the rate of photosynthetic electron transport, indicating that fluorescence is the superior remote sensing indicator for tracking acute short-term limitation of photosynthesis. Longer term adaptations of the photosynthetic apparatus involve a complex interplay of different mechanisms such as the optimization of photosynthetic efficiency at PSII and different pathways of non-photochemical energy dissipation. The quantification of these mechanisms is therefore necessary for designing a forward model to unravel the mechanism of the action of a stressor and to estimate photosynthetic CO_2 uptake rates. As suggested by this study, ancillary remote sensing variables such as vegetation indices and canopy temperature, can be used to quantify the dynamics of non-photochemical energy dissipation mechanisms, the amount and composition of photosynthetic pigments and the stomatal activity. Therefore, future missions and observations of fluorescence at large scales should consider the measurement of these variables to develop such a model and achieve a more precise assessment of changes in photosynthesis function.

ACKNOWLEDGMENTS

The authors gratefully acknowledge the financial support by the SFB/TR 32 'Pattern in Soil-Vegetation-Atmosphere Systems: Monitoring, Modelling, and Data Assimilation' project D2, funded by the Deutsche Forschungsgemeinschaft (DFG). The European Space Agency (ESA) provided additional financial support within the framework of the FLEX-EU campaign (ESA contract 4000107143/12/NL/FF/If). Data were acquired during the joint SFB/TR32 and ESA funded the HyFlex campaign. HyPlant was developed by a large-scale investment grant from the Helmholtz Association. This work was also supported by the scholarship program of CONICYT-DAAD and by the research program number 315309/CROP.SENSe.net funded by BMBF. Marin Tudoroiu was partially funded by FIRS>T (FEM International Research School) in a project supervised by the FOXLAB Joint CNR-FEM Initiative. This project has received funding from the European Union's Horizon 2020 research and innovation program under the Marie Skłodowska-Curie grant agreement No 749323 (https://ec.europa.eu/research/mariecurieactions/), held by Karolina Sakowska. The authors would like to thank to Enrico De Marchi (ROTOGREEN) and Alessandro Peressotti (University of Udine) for managing the site, Patrick Rademske (FZJ), Chiara Cilia and Andreas Burkart (FZJ, JB Hyperspectral) for support in data acquisition, Alexander Damm for discussion about the F retrieval from HyPlant data and Giulia Tagliabue for helping in the data processing.

CONFLICT OF INTEREST

The authors declare that there is no conflict of interest regarding the publication of this article.

AUTHOR CONTRIBUTIONS

R.C., F.M., M.R., D.S. and U.R. conception or design of the work. M.C., K.A., S.C., R.J., F.M., A.P., C.P., S.P., M.R., K.S., A.S., M.S. and M.T. data collection. F.P., M.C., K.A., R.J., S.M., S.P., M.R., A.S. and M.S. data analysis and interpretation. F.P. and M.C. drafting the article. F.P., M.C., K.A., G.A., S.C., R.C., R.J., S.M., F.M., A.P., C.P., S.P., M.R., K.S., A.S., M.T. and U.R. critical revision of the article.

ORCID

Francisco Pinto https://orcid.org/0000-0003-3000-9084
Karolina Sakowska https://orcid.org/0000-0003-4186-2558

REFERENCES

Ač, A., Malenovský, Z., Olejníčková, J., Gallé, A., Rascher, U., & Mohammed, G. (2015). Meta-analysis assessing potential of steady-state chlorophyll fluorescence for remote sensing detection of plant water, temperature and nitrogen stress. *Remote Sensing of Environment*, *168*, 420–436.

Agati, G. (1998). Response of the in vivo chlorophyll fluorescence spectrum to environmental factors and laser excitation wavelength. *Pure and Applied Optics*, *7*, 797–807.

Alonso, L., Gomez-Chova, L., Vila-Frances, J., Amoros-Lopez, J., Guanter, L., Calpe, J., & Moreno, J. (2008). Improved Fraunhofer line discrimination method for vegetation fluorescence quantification. *IEEE Geoscience and Remote Sensing Letters*, *5*, 620–624.

Alonso, L., Van Wittenberghe, S., Amorós-López, J., Vila-Francés, J., Gómez-Chova, L., & Moreno, J. (2017). Diurnal cycle relationships between passive fluorescence, PRI and NPQ of vegetation in a controlled stress experiment. *Remote Sensing*, *9*, 770.

Bandopadhyay, S., Rastogi, A., Rascher, U., Rademske, P., Schickling, A., Cogliati, S., … Juszczak, R. (2019). Hyplant-derived sun-induced fluorescence—A new opportunity to disentangle complex vegetation signals from diverse vegetation types. *Remote Sensing*, *11*, 1691.

Berni, J., Zarco-Tejada, P. J., Suarez, L., & Fereres, E. (2009). Thermal and narrowband multispectral remote sensing for vegetation monitoring from an unmanned aerial vehicle. *IEEE Transactions on Geoscience and Remote Sensing*, *47*, 722–738.

Buschmann, C. (2007). Variability and application of the chlorophyll fluorescence emission ratio red/far-red of leaves. *Photosynthesis Research*, *92*, 261–271.

Byrne, B., Wunch, D., Jones, D. B. A., Strong, K., Deng, F., Baker, I., … Roehl, C. M. (2018). Evaluating GPP and respiration estimates over northern midlatitude ecosystems using solar-induced fluorescence and atmospheric CO 2 measurements. *Journal of Geophysical Research: Biogeosciences*, *123*, 2976–2997.

Calderón, R., Navas-Cortés, J., & Zarco-Tejada, P. (2015). Early detection and quantification of Verticillium wilt in olive using Hyperspectral and thermal imagery over large areas. *Remote Sensing*, *7*, 5584–5610.

Calderón, R., Navas-Cortés, J. A., Lucena, C., & Zarco-Tejada, P. J. (2013). High-resolution airborne hyperspectral and thermal imagery for early detection of Verticillium wilt of olive using fluorescence, temperature and narrow-band spectral indices. *Remote Sensing of Environment*, *139*, 231–245.

Carter, G. A., Jones, J. H., Mitchell, R. J., & Brewer, C. H. (1996). Detection of solar-excited chlorophyll a fluorescence and leaf photosynthetic capacity using a fraunhofer line radiometer. *Remote Sensing of Environment*, *55*, 89–92.

Celesti, M., van der Tol, C., Cogliati, S., Panigada, C., Yang, P., Pinto, F., … Rossini, M. (2018). Exploring the physiological information of sun-induced chlorophyll fluorescence through radiative transfer model inversion. *Remote Sensing of Environment*, *215*, 97–108.

Cogliati, S., Rossini, M., Julitta, T., Meroni, M., Schickling, A., Burkart, A., … Colombo, R. (2015). Continuous and long-term measurements of reflectance and sun-induced chlorophyll fluorescence by using novel automated field spectroscopy systems. *Remote Sensing of Environment*, *164*, 270–281.

Cogliati, S., Verhoef, W., Kraft, S., Sabater, N., Alonso, L., Vicent, J., … Colombo, R. (2015). Retrieval of sun-induced fluorescence using advanced spectral fitting methods. *Remote Sensing of Environment*, *169*, 344–357.

Damm, A., Guanter, L., Laurent, V. C. E., Schaepman, M. E., Schickling, A., & Rascher, U. (2014). FLD-based retrieval of sun-induced chlorophyll fluorescence from medium spectral resolution airborne spectroscopy data. *Remote Sensing of Environment*, *147*, 256–266.

Damm, A., Guanter, L., Verhoef, W., Schläpfer, D., Garbari, S., & Schaepman, M. E. (2015). Impact of varying irradiance on vegetation indices and chlorophyll fluorescence derived from spectroscopy data. *Remote Sensing of Environment*, *156*, 202–215.

Dash, J., & Curran, P. J. (2004). International journal of remote sensing the MERIS terrestrial chlorophyll index the MERIS terrestrial chlorophyll index. *International Journal of Remote Sensing*, *2523*, 5403–5413.

Daumard, F., Champagne, S., Fournier, A., Goulas, Y., Ounis, A., Hanocq, J. F., & Moya, I. (2010). A field platform for continuous measurement of canopy fluorescence. *IEEE Transactions on Geoscience and Remote Sensing*, *48*, 3358–3368.

Dobrowski, S. Z., Pushnik, J. C., Zarco-Tejada, P. J., & Ustin, S. L. (2005). Simple reflectance indices track heat and water stress-induced changes in steady-state chlorophyll fluorescence at the canopy scale. *Remote Sensing of Environment*, *97*, 403–414.

Drusch, M., Moreno, J., Del Bello, U., Franco, R., Goulas, Y., Huth, A., … Verhoef, W. (2017). The FLuorescence EXplorer Mission concept—ESA's earth Explorer 8. *IEEE Transactions on Geoscience and Remote Sensing*, *55*, 1273–1284.

Ducruet, J.-M., Sixto, H., & Garcia-Baudin, J.-M. (1993). Using chlorophyll fluorescence induction for a quantitative detoxification assay with metribuzin and chlorotoluron in excised wheat (Triticum aestivum and *Triticum durum*) leaves. *Pesticide Science*, *38*, 295–301.

Filella, I., Amaro, T., Araus, J. L., & Peñuelas, J. (1996). Relationship between photosynthetic radiation-use efficiency of barley canopies and the photochemical reflectance index (PRI). *Physiologia Plantarum*, *96*, 211–216.

Filella, I., Porcar-Castell, A., Munné-Bosch, S., Bäck, J., Garbulsky, M. F., & Peñuelas, J. (2009). PRI assessment of long-term changes in carotenoids/chlorophyll ratio and short-term changes in de-epoxidation state of the xanthophyll cycle. *International Journal of Remote Sensing*, *30*, 4443–4455.

Flexas, J., Escalona, J. M., Evain, S., Gulias, J., Moya, I., Osmond, C. B., & Medrano, H. (2002). Steady-state chlorophyll fluorescence (Fs) measurements as a tool to follow variations of net CO2 assimilation and stomatal conductance during water-stress in C3 plants. *Physiologia Plantarum*, *114*, 231–240.

Frankenberg, C., Butz, A., & Toon, G. C. (2011). Disentangling chlorophyll fluorescence from atmospheric scattering effects in O 2 A-band spectra of reflected sun-light. *Geophysical Research Letters*, *38*, L03801.

Frankenberg, C., Fisher, J. B., Worden, J., Badgley, G., Saatchi, S. S., Lee, J.-E., … Yokota, T. (2011). New global observations of the terrestrial carbon cycle from GOSAT: Patterns of plant fluorescence with gross primary productivity. *Geophysical Research Letters*, *38*.

Fuentes, S., De Bei, R., Pech, J., & Tyerman, S. (2012). Computational water stress indices obtained from thermal image analysis of grapevine canopies. *Irrigation Science*, *30*, 523–536.

Gamon, J. A., Field, C. B., Bilger, W., Björkman, O., Fredeen, A. L., & Peñuelas, J. (1990). Remote sensing of the xanthophyll cycle and chlorophyll fluorescence in sunflower leaves and canopies. *Oecologia*, *85*, 1–7.

Gamon, J. A., Peñuelas, J., & Field, C. B. (1992). A narrow-waveband spectral index that tracks diurnal changes in photosynthetic efficiency. *Remote Sensing of Environment*, *41*, 35–44.

Garbulsky, M. F., Peñuelas, J., Gamon, J., Inoue, Y., & Filella, I. (2011). The photochemical reflectance index (PRI) and the remote sensing of leaf, canopy and ecosystem radiation use efficiencies. A review and meta-analysis. *Remote Sensing of Environment*, *115*, 281–297.

Gitelson, A. A., Gamon, J. A., & Solovchenko, A. (2017). Multiple drivers of seasonal change in PRI: Implications for photosynthesis 1. Leaf level. *Remote Sensing of Environment*, *191*, 110–116.

Guanter, L. (2007). *New algorithms for atmospheric correction and retrieval of biophysical parameters in earth observation. application to ENVISAT/MERIS data*. Department de Fisica de la Terra i Termodinàmica, Universitat de València, Valencia, Spain

Guanter, L., Frankenberg, C., Dudhia, A., Lewis, P. E., Gómez-Dans, J., Kuze, A., … Grainger, R. G. (2012). Retrieval and global assessment of terrestrial chlorophyll fluorescence from GOSAT space measurements. *Remote Sensing of Environment*, *121*, 236–251.

Guanter, L., Zhang, Y., Jung, M., Joiner, J., Voigt, M., Berry, J. A., … Griffis, T. J. (2014). Global and time-resolved monitoring of crop photosynthesis with chlorophyll fluorescence. *Proceedings of the National Academy of Sciences of the United States of America*, *111*, E1327–E1333.

Haboudane, D., Miller, J. R., Tremblay, N., Zarco-Tejada, P. J., & Dextraze, L. (2002). Integrated narrow-band vegetation indices for prediction of crop chlorophyll content for application to precision agriculture, *81*, 416–426.

Hall, L. M., Moss, S. R., & Powles, S. B. (1995). Mechanism of resistance to chlorotoluron in two biotypes of the grass weed *Alopecurus myosuroides*. *Pesticide Biochemistry and Physiology*, *53*, 180–192.

Hernández-Clemente, R., North, P. R. J., Hornero, A., & Zarco-Tejada, P. J. (2017). Assessing the effects of forest health on sun-induced chlorophyll fluorescence using the FluorFLIGHT 3-D radiative transfer model to account for forest structure. *Remote Sensing of Environment*, *193*, 165–179.

Hoffmann, M., Jurisch, N., Albiac, B. E., Hagemann, U., Drösler, M., Sommer, M., & Augustin, J. (2015). Automated modeling of ecosystem

CO2 fluxes based on periodic closed chamber measurements: A standardized conceptual and practical approach. *Agricultural and Forest Meteorology*, *200*, 30–45.

Hyde, R. J., Hallahan, D. L., & Bowyer, J. R. (1996). Chlorotoluron metabolism in leaves of resistant and susceptible biotypes of the grass weed *Alopecurus myosuroides*. *Pesticide Science*, *47*, 185–190.

Joiner, J., Yoshida, Y., Guanter, L., & Middleton, E. M. (2016). New methods for the retrieval of chlorophyll red fluorescence from hyperspectral satellite instruments: Simulations and application to GOME-2 and SCIAMACHY. *Atmospheric Measurement Techniques*, *9*, 3939–3967.

Joiner, J., Yoshida, Y., Vasilkov, A. P., Yoshida, Y., Corp, L. A., & Middleton, E. M. (2011). First observations of global and seasonal terrestrial chlorophyll fluorescence from space. *Biogeosciences*, *8*, 637–651.

Juszczak, R., Humphreys, E., Acosta, M., Michalak-Galczewska, M., Kayzer, D., & Olejnik, J. (2013). Ecosystem respiration in a heterogeneous temperate peatland and its sensitivity to peat temperature and water table depth. *Plant and Soil*, *366*, 505–520.

Juszczak, R., Uździcka, B., Stróżecki, M., & Sakowska, K. (2018). Improving remote estimation of winter crops gross ecosystem production by inclusion of leaf area index in a spectral model. *PeerJ*, *6*, e5613.

Lee, J.-E., Frankenberg, C., van der Tol, C., Berry, J. a., Guanter, L., Boyce, C. K., … Saatchi, S. (2013). Forest productivity and water stress in Amazonia: Observations from GOSAT chlorophyll fluorescence. *Proceedings of the Royal Society B: Biological Sciences*, *280*, 20130171–20130171.

Li, Y., Zhou, J., Kinzelbach, W., Cheng, G., Li, X., & Zhao, W. (2013). Coupling a SVAT heat and water flow model, a stomatal-photosynthesis model and a crop growth model to simulate energy, water and carbon fluxes in an irrigated maize ecosystem. *Agricultural and Forest Meteorology*, *176*, 10–24.

Li, Z.-L., Tang, B.-H., Wu, H., Ren, H., Yan, G., Wan, Z., … Sobrino, J. A. (2013). Satellite-derived land surface temperature: Current status and perspectives. *Remote Sensing of Environment*, *131*, 14–37.

Lichtenthaler, H. K., & Buschmann, C. (2001). Chlorophylls and carotenoids: Measurement and characterization by UV-VIS spectroscopy. *Current protocols in food analytical chemistry*, 1, F4.2.1–F4.3.8.

Lichtenthaler, H. K., & Rinderle, U. (1988). The role of chlorophyll fluorescence in the detection of stress conditions in plants. *C R C Critical Reviews in Analytical Chemistry*, *19*, S29–S85.

Magney, T. S., Bowling, D. R., Logan, B. A., Grossmann, K., Stutz, J., Blanken, P. D., … Frankenberg, C. (2019). Mechanistic evidence for tracking the seasonality of photosynthesis with solar-induced fluorescence. *Proceedings of the National Academy of Sciences of the United States of America*, *116*, 201900278.

Maier, S. W., Günther, K. P., & Stellmes, M. (2003). Sun-induced fluorescence: A new tool for precision farming. In: *Digital imaging and spectral techniques: applications to precision agriculture and crop physiology*, *ASA Special Publication 66*. J.Schepers, T. Van Toai (editors). Madison WI: ASA, CSSA and SSA (publisher). (pp. 209–222).

Meroni, M., & Colombo, R. (2006). Leaf level detection of solar induced chlorophyll fluorescence by means of a subnanometer resolution spectroradiometer. *Remote Sensing of Environment*, *103*, 438–448.

Meroni, M., & Colombo, R. (2009). 3S: A novel program for field spectroscopy. *Computers and Geosciences*, *35*, 1491–1496.

Meroni, M., Rossini, M., Guanter, L., Alonso, L., Rascher, U., Colombo, R., & Moreno, J. (2009). Remote sensing of solar-induced chlorophyll fluorescence: Review of methods and applications. *Remote Sensing of Environment*, *113*, 2037–2051.

Meroni, M., Rossini, M., Picchi, V., Panigada, C., Cogliati, S., Nali, C., & Colombo, R. (2008). Assessing steady-state fluorescence and PRI from hyperspectral proximal sensing as early indicators of plant stress: The case of ozone exposure. *Sensors*, *8*, 1740–1754.

Mohammed, G. H., Colombo, R., Middleton, E. M., Rascher, U., van der Tol, C., Nedbal, L., … Zarco-Tejada, P. J. (2019). Remote sensing of solar-induced chlorophyll fluorescence (SIF) in vegetation: 50 years of progress. *Remote Sensing of Environment*, *231*, 111177.

Müller, P., Li, X.-P. P., Niyogi, K. K., & Muller, P. (2001). Non-photochemical quenching. A response to excess light energy. *Plant Physiology*, *125*, 1558–1566.

Murakami, K., & Ibaraki, Y. (2019). Time course of the photochemical reflectance index during photosynthetic induction: Its relationship with the photochemical yield of photosystem II. *Physiologia Plantarum*, *165*, 524–536.

Osmond, C. B. (1994). What is photoinhibition? Some insights from comparisons of shade and sun plants. In N. R. Baker & J. R. Bowyer (Eds.), *Photoinhibition of photosynthesis: From molecular mechanisms to the field* (pp. 1–24). Oxford, England: BIOS Scientific.

Panigada, C., Rossini, M., Meroni, M., Cilia, C., Busetto, L., Amaducci, S., … Colombo, R. (2014). Fluorescence, PRI and canopy temperature for water stress detection in cereal crops. *International Journal of Applied Earth Observation and Geoinformation*, *30*, 167–178.

Panigada, C., Rossini, M., Meroni, M., Marzuoli, R., Gerosa, G., & Colombo, R. (2009). Indicators of ozone effects on *Fagus sylvatica* L. by means of spectroradiometric measurements. *Italian Journal of Remote Sensing*, *41*, 3–20.

Papageorgiou, G. C., & Govindjee. (2004). *Chlorophyll a fluorescence: a signature of photosynthesis*. Dordrecht: Kluwer Academic.

Perez-Priego, O., Guan, J., Rossini, M., Fava, F., Wutzler, T., Moreno, G., … Migliavacca, M. (2015). Sun-induced chlorophyll fluorescence and PRI improve remote sensing GPP estimates under varying nutrient availability in a typical Mediterranean savanna ecosystem. *Biogeosciences Discussions*, *12*, 11891–11934.

Pignatti, S., Lapenna, V., Palombo, A., Pascucci, S., Pergola, N., & Cuomo, V. (2011). *An advanced tool of the CNR IMAA EO facilities: Overview of the TASI-600 hyperspectral thermal spectrometer* (pp. 1–4). In 2011 3rd Workshop on Hyperspectral Image and Signal Processing: Evolution in Remote Sensing (WHISPERS). IEEE.

Pinto, F., Damm, A., Schickling, A., Panigada, C., Cogliati, S., Müller-Linow, M., … Rascher, U. (2016). Sun-induced chlorophyll fluorescence from high-resolution imaging spectroscopy data to quantify spatio-temporal patterns of photosynthetic function in crop canopies. *Plant, Cell and Environment*, *39*, 1500–1512.

Plascyk, J. A. (1975). Mk II Fraunhofer line discriminator (FLD-II) for airborne and orbital remote-sensing of solar-stimulated luminescence. *Optical Engineering*, *14*, 339–346.

Porcar-Castell, A., Garcia-Plazaola, J. I., Nichol, C. J., Kolari, P., Olascoaga, B., Kuusinen, N., … Nikinmaa, E. (2012). Physiology of the seasonal relationship between the photochemical reflectance index and photosynthetic light use efficiency. *Oecologia*, *170*, 313–323.

Porcar-Castell, A., Tyystjarvi, E., Atherton, J., van der Tol, C., Flexas, J., Pfundel, E. E., … Berry, J. A. (2014). Linking chlorophyll a fluorescence to photosynthesis for remote sensing applications: Mechanisms and challenges. *Journal of Experimental Botany*, *65*, 4065–4095.

Rascher, U., Alonso, L., Burkart, A., Cilia, C., Cogliati, S., Colombo, R., … Zemek, F. (2015). Sun-induced fluorescence—A new probe of photosynthesis: First maps from the imaging spectrometer HyPlant. *Global Change Biology*, *21*, 4673–4684.

Van Rensen, J. (1989). Herbicides interacting with photosystem II. In A. D. Dodge (Ed.), *Herbicides and plant metabolism* (p. 21). Cambridge, England: Cambridge University Press.

Ridley, S. M. (1977). Interaction of chloroplasts with inhibitors. *Plant Physiology*, *59*, 724–732.

Rossini, M., Meroni, M., Celesti, M., Cogliati, S., Julitta, T., Panigada, C., … Colombo, R. (2016). Analysis of red and far-red sun-induced chlorophyll fluorescence and their ratio in different canopies based on observed and modeled data. *Remote Sensing*, *8*, 412.

Rossini, M., Meroni, M., Migliavacca, M., Manca, G., Cogliati, S., Busetto, L., … Colombo, R. (2010). High resolution field spectroscopy measurements for estimating gross ecosystem production in a rice field. *Agricultural and Forest Meteorology*, *150*, 1283–1296.

Rossini, M., Nedbal, L., Guanter, L., Ač, A., Alonso, L., Burkart, A., … Rascher, U. (2015). Red and far red sun-induced chlorophyll fluorescence as a measure of plant photosynthesis. *Geophysical Research Letters*, *42*, 1632–1639.

Rouse, J. W., Haas, R. H., Schell, J. A., & Deering, D. W. (1974). *Monitoring vegetation systems in the Great Okains with ERTS* (Vol. **1, pp.** 325–333). Third Earth Resources Technology Satellite-1 Symposium, Washington, D.C. (1973), *351*, 309.

Ruban, A. V., & Horton, P. (1999). The xanthophyll cycle modulates the kinetics of nonphotochemical energy dissipation in isolated light-harvesting complexes, intact chloroplasts, and leaves of spinach. *Plant Physiology*, *119*, 531–542.

Santini, F., Palombo, A., Dekker, R. J., Pignatti, S., Pascucci, S., & Schwering, P. B. W. (2014). Advanced anomalous pixel correction algorithms for hyperspectral thermal infrared data: The TASI-600 case study. *IEEE Journal of Selected Topics in Applied Earth Observations and Remote Sensing*, *7*, 2393–2404.

Schickling, A., Matveeva, M., Damm, A., Schween, J. H., Wahner, A., Graf, A., … Rascher, U. (2016). Combining sun-induced chlorophyll fluorescence and photochemical reflectance index improves diurnal modeling of gross primary productivity. *Remote Sensing*, *8*, 574.

Schreiber, U. (1986). Detection of rapid induction kinetics with a new type of high-frequency modulated chlorophyll fluorometer. *Photosynthesis Research*, *9*, 261–272.

Song, L., Guanter, L., Guan, K., You, L., Huete, A., Ju, W., & Zhang, Y. (2018). Satellite sun-induced chlorophyll fluorescence detects early response of winter wheat to heat stress in the Indian Indo-Gangetic plains. *Global Change Biology*, *24*, 4023–4037.

Wang, W.-H., He, E.-M., Guo, Y., Tong, Q.-X., & Zheng, H.-L. (2016). Chloroplast calcium and ROS signaling networks potentially facilitate the primed state for stomatal closure under multiple stresses. *Environmental and Experimental Botany*, *122*, 85–93.

Weed Science Society of America. (2020). Herbicide site of action (SOA) classification list. Retrieved from: http://wssa.net/wssa/weed/herbicides/

Wieneke, S., Ahrends, H., Damm, A., Pinto, F., Stadler, A., Rossini, M., & Rascher, U. (2016). Airborne based spectroscopy of red and far-red sun-induced chlorophyll fluorescence: Implications for improved estimates of gross primary productivity. *Remote Sensing of Environment*, *184*, 654–667.

Wieneke, S., Burkart, A., Cendrero-Mateo, M. P., Julitta, T., Rossini, M., Schickling, A., … Rascher, U. (2018). Linking photosynthesis and sun-induced fluorescence at sub-daily to seasonal scales. *Remote Sensing of Environment*, *219*, 247–258.

Wohlfahrt, G., Gerdel, K., Migliavacca, M., Rotenberg, E., Tatarinov, F., Müller, J., … Yakir, D. (2018). Sun-induced fluorescence and gross primary productivity during a heat wave. *Scientific Reports*, *8*, 14169.

Xu, S., Liu, Z., Zhao, L., Zhao, H., & Ren, S. (2018). Diurnal response of sun-induced fluorescence and PRI to water stress in maize using a near-surface remote sensing platform. *Remote Sensing*, *10*, 1510.

Yang, P., van der Tol, C., Verhoef, W., Damm, A., Schickling, A., Kraska, T., … Rascher, U. (2019). Using reflectance to explain vegetation biochemical and structural effects on sun-induced chlorophyll fluorescence. *Remote Sensing of Environment*, *231*, 110996.

Young, S. J. (1998). In scene atmospheric compensation: Application to SEBASS data collected at the ARM site. Part II. Aerospace Report ATR-99 (8407), Part II.

Zarco-Tejada, P. J., Camino, C., Beck, P. S. A., Calderon, R., Hornero, A., Hernández-Clemente, R., … Navas-Cortes, J. A. (2018). Previsual symptoms of *Xylella fastidiosa* infection revealed in spectral plant-trait alterations. *Nature Plants*, *4*, 432–439.

Zarco-Tejada, P. J., González-Dugo, V., & Berni, J. A. J. (2012). Fluorescence, temperature and narrow-band indices acquired from a UAV platform for water stress detection using a micro-hyperspectral imager and a thermal camera. *Remote Sensing of Environment*, *117*, 322–337.

Zhao, F., Li, R., Verhoef, W., Cogliati, S., Liu, X., Huang, Y., … Huang, J. (2018). Reconstruction of the full spectrum of solar-induced chlorophyll fluorescence: Intercomparison study for a novel method. *Remote Sensing of Environment*, *219*, 233–246.

SUPPORTING INFORMATION

Additional supporting information may be found online in the Supporting Information section at the end of this article.

How to cite this article: Pinto F, Celesti M, Acebron K, et al. Dynamics of sun-induced chlorophyll fluorescence and reflectance to detect stress-induced variations in canopy photosynthesis. *Plant Cell Environ*. 2020;43:1637–1654. https://doi.org/10.1111/pce.13754